Processes going on in Nonfailed Rod during Normal Operation

Volume I

Author

Charles Patterson
Clovis, California, USA

with contributions from

Friedrich Garzarolli
Fürth, Germany

Reviewed by

Ron Adamson
Zircology Plus, Fremont, California, USA

A.N.T. INTERNATIONAL®

Advanced Nuclear Technology International
Analysvägen 5, SE-435 33 Mölnlycke
Sweden

info@antinternational.com
www.antinternational.com

Ecolabelled printed matter, 441 799

Disclaimer

The information presented in this report has been compiled and analysed by Advanced Nuclear Technology International Europe AB (ANT International®) and its subcontractors. ANT International has exercised due diligence in this work, but does not warrant the accuracy or completeness of the information. ANT International does not assume any responsibility for any consequences as a result of the use of the information for any party, except a warranty for reasonable technical skill, which is limited to the amount paid for this assignment by each ZIRAT/IZNA programme member.

Contents

1 Introduction

The use of uranium dioxide as a material to generate and conduct heat in water reactors appears, at first glance, to be an odd choice. It is a ceramic compound in which oxygen atoms displace uranium atoms and decrease the amount of energy that can be generated per unit volume. Its thermal conductivity is also markedly lower than that of metallic uranium and becomes even lower with increasing temperature; e.g., the thermal conductivity of UO_2 is about 1/10 of the conductivity of metallic uranium at temperatures typical of water reactors. Low thermal conductivity increases the temperature of and energy stored within the fuel, thereby exacerbating heat removal under emergency conditions and arguing against the use of UO_2 as a fuel material. As with most engineering decisions, however, the choice of UO_2 as fuel for water reactors involves a number of conflicting factors.

A primary consideration in the selection of UO_2 as the fuel material is the use of water as the coolant. Metallic uranium corrodes rapidly in water at temperatures typical of the primary system; e.g., ≥300 °C. Such corrosion can lead to significant fuel degradation and unacceptable transport of radioactive material throughout the reactor in cases where cladding, end plug or welding failures exposed the fuel to the coolant.

Other important factors in the selection of UO_2 for water cooled reactors rather than metallic uranium involve chemical and dimensional stability. Metallic uranium can react with common cladding materials, thereby degrading their functional performance. Metallic uranium also undergoes dimensional changes that adversely affects its use as a fuel material. Part of these dimensional changes comes from transitions in crystallographic structure and physical state; viz., change from the orthorhombic α-phase to tetragonal β-phase at 665 °C, from the β-phase to the body-centred cubic γ-phase at 770 °C and melting at 1130 °C. These phase transformations can be controlled by the addition of small amounts of alloying elements to stabilize either the β-phase or the γ-phase or by alloying uranium with aluminium to form UAl_2, UAl_3 or UAl_4. Solid-state phase transitions in metallic uranium produce dimensional instabilities without changes in density. But, the primary dimensional problem with metallic uranium comes from the accumulation of Fission Products (FPs). That is, the nucleation and growth of fission gas bubbles leads to gaseous swelling which increases with exposure and temperature. The accumulation of solid FPs also leads to swelling due to the lower density of the FPs and their decay products relative to the density of the uranium atoms from which they originated. The accumulation of FPs produces volumetric expansion that can become significant at temperatures above 350 °C. The use of UO_2 greatly mitigates issues related with both chemical and dimensional stability.

Materials other than metallic uranium have also been considered as a fuel material. Uranium Carbide (UC) and Uranium Nitride (UN), conduct heat much more readily than UO_2 and are used in other types of nuclear reactors. Both compounds also address the chemical stability and corrosion issues associated with metallic uranium to varying degrees. For reference, the chemical and physical properties of UC and UN as related to water applications are compared to those of metallic uranium and UO_2 in Table 1-1. As with metallic uranium, the primary advantage of UO_2 over UC and UN in water cooled reactors is its stability in a water environment.

Table 1-1: Properties of uranium compounds as related to water reactor applications, after Garzarolli [Rudling et al, 2007]

Property	Uranium	UO_2	UC	UN
A. Chemical				
Free energy of formation at 1000 °K (Kcal/mole)	-	-218.2	-25.2	-47
Corrosion resistance in water	Very poor	Excellent	Very poor	Poor
Compatibility with clad materials	Reacts with normal clad	Excellent	Variable	Variable
Thermal stability	Phase change at 665 and 770 °C	Good	Good in reducing atmosphere	Good, decomposes at 2600 °C
B. Physical				
Uranium (metal) density (g/cm^3)	19.04	9.65	12.97	13.52
Theoretical Density (T.D.) (g/cm^3)		10.96		
Melting point (°C)	1132	2865	2850	2850
Thermal conductivity W/cm/K	0.28 at 430 °C	0.03 at 1000 °C	0.25 at 100-700 °C	0.2 at 750 °C

As a result, UO_2 has become the standard fuel material for water cooled reactors and is the subject of this Special Topical Report (STR). The behaviour of sintered UO_2 fuel and, to a lesser extent, of mixed uranium-plutonium dioxide fuel ($(U,Pu)O_2$ or, more commonly, Mixed Oxide (MOX)) is reviewed in this STR. The objective of the report is to provide a basis for related reviews of zirconium alloys within the ZIRconium Alloy Technology (ZIRAT) and Information on Zirconium Alloys (IZNA) programs by identifying aspects of fuel behaviour that affect the performance and reliability of fuel cladding and integral fuel rods.

Volume I of the STR focuses on the behaviour of water reactor fuel during normal and near-normal operating conditions. The principal subject, shown schematically in Figure 1-1, is sintered, cylindrical pellets of UO_2 or MOX that are encased in tubes constructed of a zirconium alloy, sealed with zirconium alloy end plugs and filled with an inert gas such as helium. The report also addresses the effects of burnable neutron absorbers (poisons) and briefly summarizes the observed and postulated effects of pellet additives that are being introduced to enhance the performance of power-reactor fuel. Fuel behaviour is considered during normal and near-normal operating conditions as a means for limiting the size of the Report. Fuel behaviour during accident conditions is covered separately in Volume II of the ZRAT15 STR and as part of other reports; e.g., [Adamson et al, 2003/2004], [Rudling et al, 2004/2005], [Adamson et al, 2006/2007] and [Rudling et al, 2007].

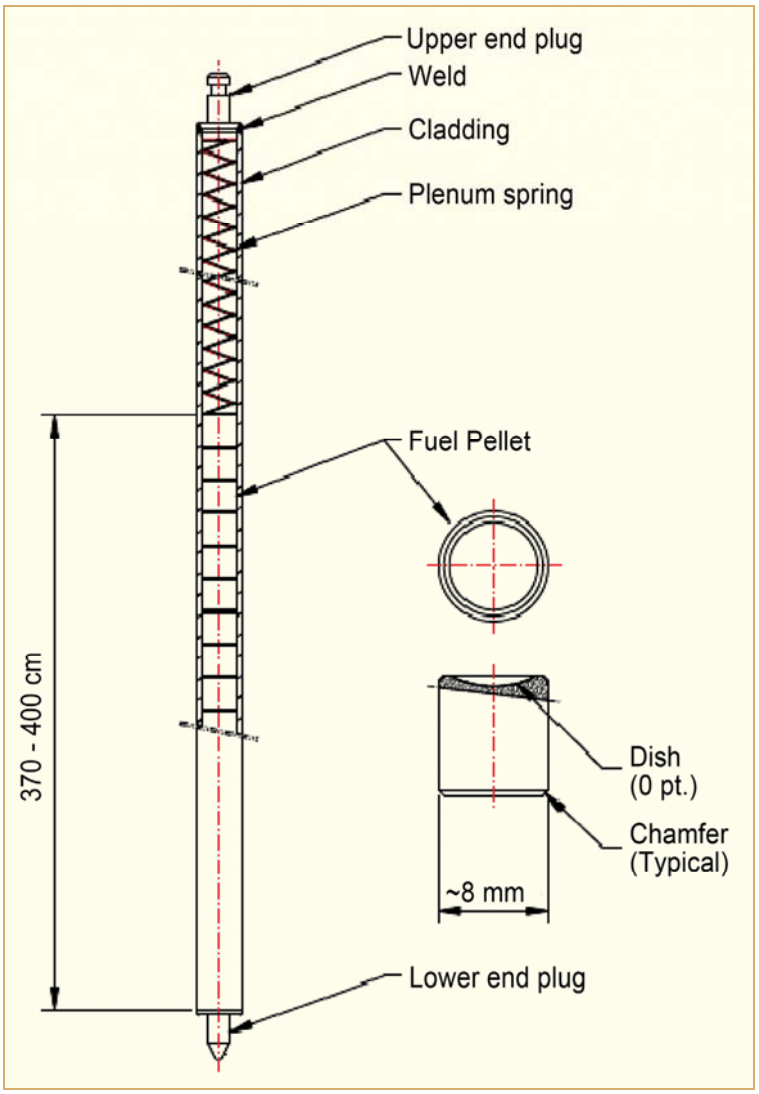

Figure 1-1: Schematic diagram of water reactor fuel rod and sintered, cylindrical fuel pellet.

The report begins with a review of the fission process. It then covers the chemical and structural properties of UO_2 as related to the thermal and mechanical behaviour of fuel pellets, heat transfer, thermal and mechanical properties and the effects of in-reactor operation on fuel behaviour and the interaction of pellets and cladding. For reference, these processes and their interaction are summarized in Figure 1-2. Although this figure is somewhat confusing (and looks like it might have been created on a bar napkin after a long technical seminar), it is a well conceived and relatively complete representation of factors that affect the in-reactor performance of nuclear fuel. The process diagram is provided as a road map for material presented the following sections of this report. As noted earlier, the overall objective of the STR is to identify aspects of fuel behaviour relevant to the performance of zirconium-based fuel cladding.

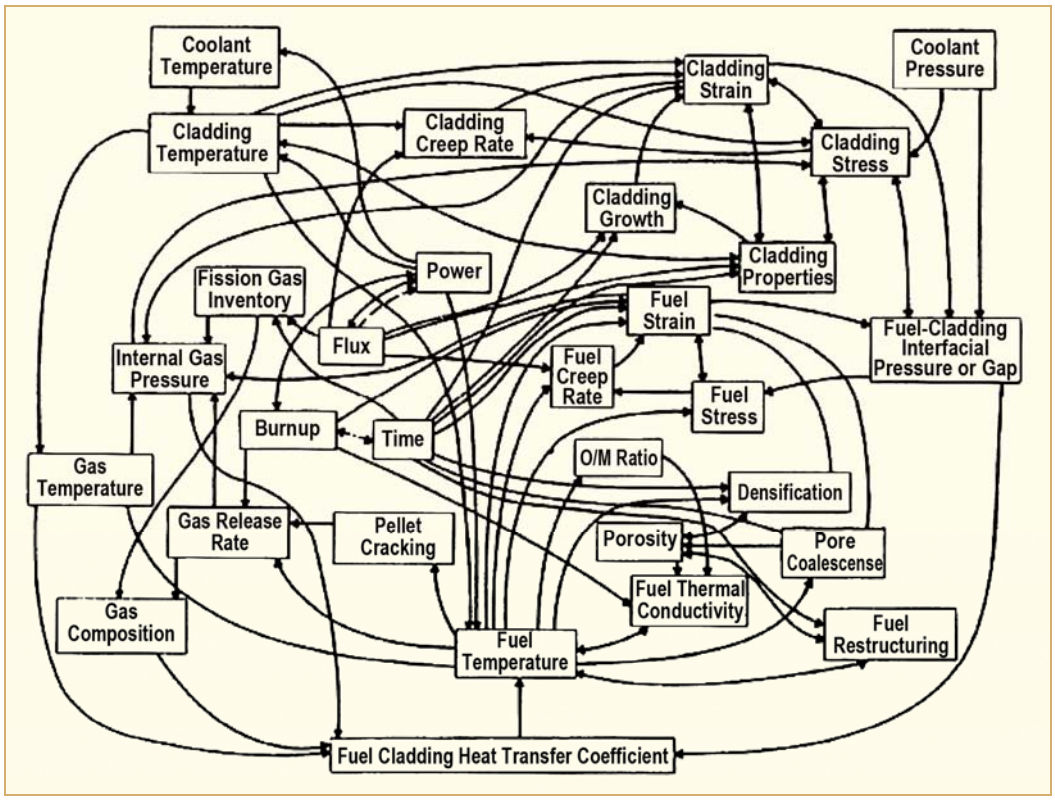

Figure 1-2: Primary processes in an operating fuel rod and their interactions [Mohr et al, 1976][1].

As a general comment, "burnup" in Figure 1-2 is usually expressed in terms of the energy generated per unit mass of fuel; e.g., gigawatt-days per metric ton of uranium, GWd/MTU, or equivalently as megawatt-days per kilogram of uranium, MWd/kgU. For MOX fuel, burnup is given in terms of energy production per unit mass of metal or per unit mass of initial heavy metal; e.g., GWd/MTHM. In some areas of fuel technology, burnup is expressed in terms of the fraction of initial heavy atoms that have fissioned; i.e., at.% burnup or Fissions per Initial Metal Atom (FIMA). Atomic-percent burnup is related to energy-production burnup by means of the energy yield per fission, which is discussed in the next section.

[1] This figure was presented by Mohr and co-workers in the cited reference. However, it is attributed by Mohr to G.R. Horn of the Babcock & Wilcox Company, Lynchburg, VA with a note that the he was deceased at the time of publication. The figure is believed to have come from Horn and appears not to have been documented in accessible sources prior to the report by Mohr, et al.

2 Fission process

The absorption of a neutron by certain nuclei of high atomic number can lead to a fission event. When fission takes place, the excited compound nucleus formed after absorption of a neutron breaks up into two lighter nuclei, called fission fragments. This process is shown schematically in Figure 2-1. Three nuclides with sufficient stability to survive for a long time, namely ^{233}U, ^{235}U, and ^{239}Pu, are fissionable by neutrons of all energies. Of these nuclides, ^{235}U is the only one that occurs in nature; the other two are produced by neutron absorption followed by radioactive decay from ^{232}Th and ^{238}U, respectively. As discussed later in this section, the capture of epithermal neutrons by ^{238}U, decay, subsequent transmutations of ^{239}Pu and fissioning of ^{239}Pu and ^{241}Pu play an important role in the in-reactor behaviour and energy generation by water reactor fuel.

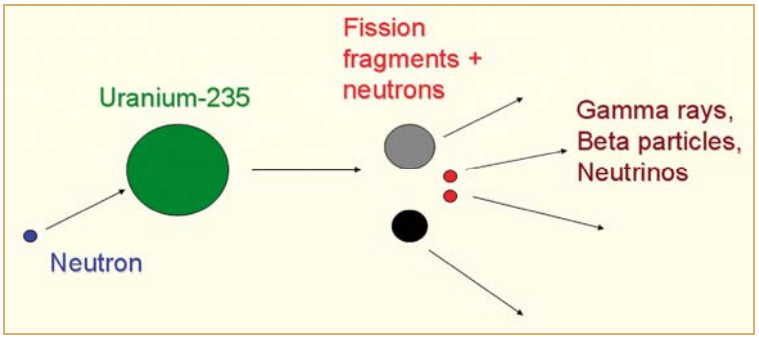

Figure 2-1: Schematic description of fission process.

The liberation of neutrons in the fission reaction can be explained as follows. In the compound nucleus ^{236}U, which is formed when a ^{235}U nucleus captures a neutron, the ratio of neutrons to protons is nearly 1.57. This nucleus is unstable and splits into two parts, with a light group of mass numbers centred at 95 and a heavy group centred at 140. The separation of the compound nucleus ^{236}U into fission fragments is a statistical process, with the fragments distributed around the light and heavy peaks. These fission fragment nuclei are unstable due to an overly large neutron-to-proton ratio. Consequently, if these nuclei produced in fission have sufficient excitation energy, they can expel neutrons, thereby tending to become more stable. The actual number of neutrons released in this manner is too small, however, to confer stability on the resulting fission fragments. Most of the latter still have too high a ratio of neutrons to protons, and will consequently be radioactive, exhibiting negative beta decay at varying rates. The total production of neutrons is also a statistical process which depends on the fissionable isotope and the energy of the captured neutron. The average number of neutrons produced by each fission is approximately 2.4 and 2.9 for ^{235}U and ^{239}Pu, respectively, following the capture of a thermal energy neutron; e.g., 0.025 eV.

Although this STR focuses on the thermal and mechanical behaviour of fuel material, a brief diversion into nuclear physics is needed as background for conditions that arise during operation. To begin, a fission event in a thermal spectrum reactor generates neutrons with a wide range of energies. An example of the neutron spectrum from fissioning of ^{235}U is shown in Figure 2-2. High energy neutrons (> 1 MeV) are typically significant in physical processes such as irradiation damage and creep of fuel cladding. Lower energy neutrons are significant to the fissioning of the fuel itself. Note that the distinction between high energy and low energy is somewhat arbitrary relative to effects of neutrons on the structure of fuel and cladding materials. Ignoring the atomic displacements that come from capture and decay, displacements caused by the collision of neutrons with lattice atoms varies with factors such as atomic mass, neutron energy, energy transfer parameter and collision cross section. The value noted above for high energy neutrons (> 1 MeV) is a common threshold for evaluating material behaviour relative to fast neutron fluence even though collision displacements can begin with neutron energies of 0.1 MeV.

A neutron can interact with material in a water reactor in several ways; e.g., by scattering collisions, which can be elastic or inelastic, and by capture, which can lead to absorption of the neutron or to fissioning of the target nucleus. As shown in Figure 2-3 and Figure 2-4, the fraction of the neutrons reacting with a given target nucleus (as expressed by the respective fission cross-section) depends strongly on the energy of the incident neutrons. Similar relationships apply to scattering and absorption reactions. Typical values of the scattering, absorption and fission cross-sections are summarized in Table 2-1 for neutron energies relevant to water reactors.

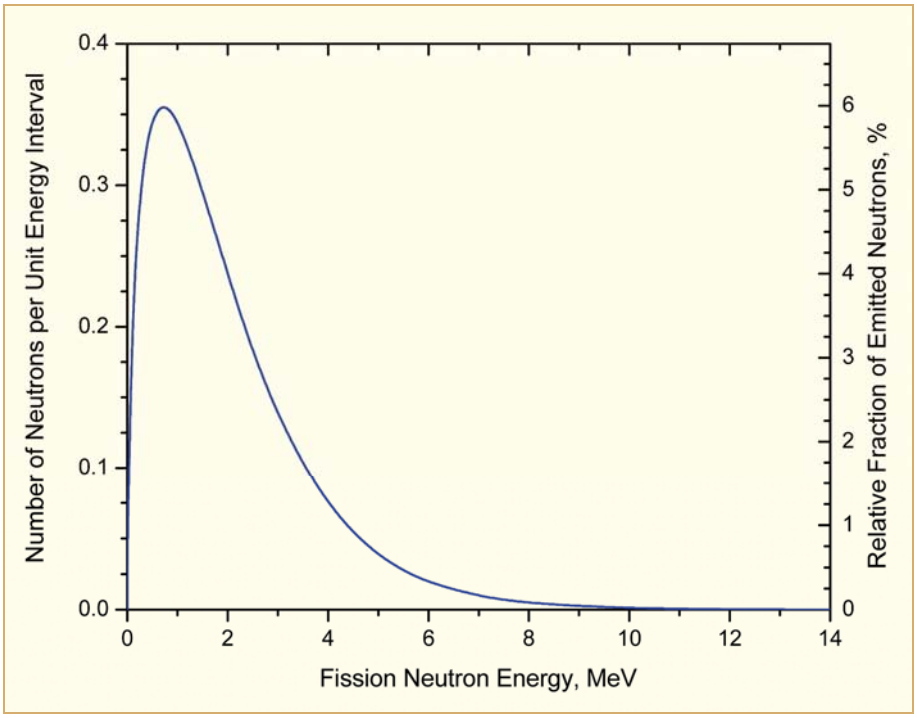

Figure 2-2: Neutron spectrum from the fissioning of ^{235}U, after [Glasstone & Sesonske, 1967].

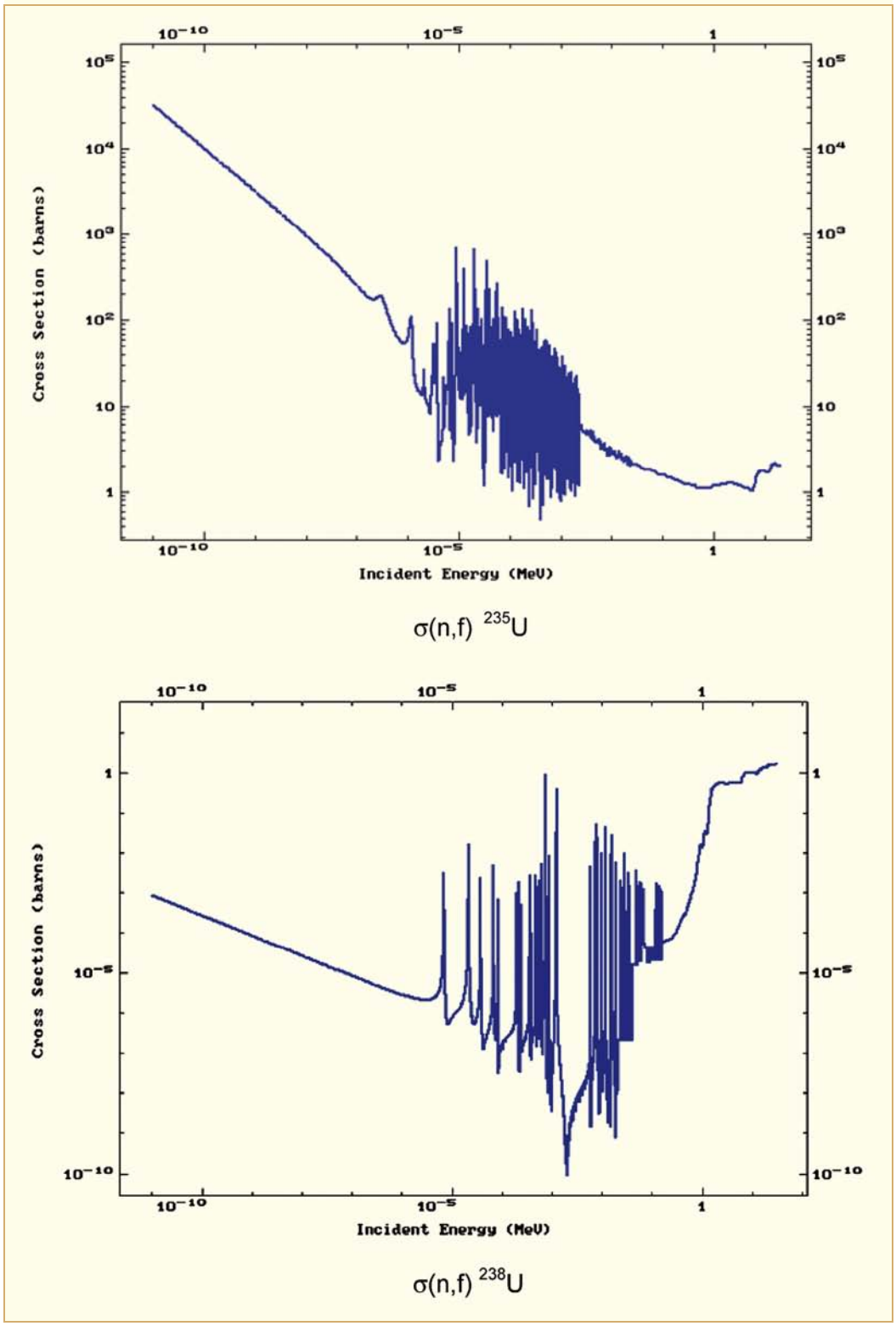

Figure 2-3: Fission cross-sections relative to neutron energy for ^{235}U and ^{238}U. NB: Note differences in cross-section scales [NNDC[2], 2010].

[2] National Nuclear Data Center

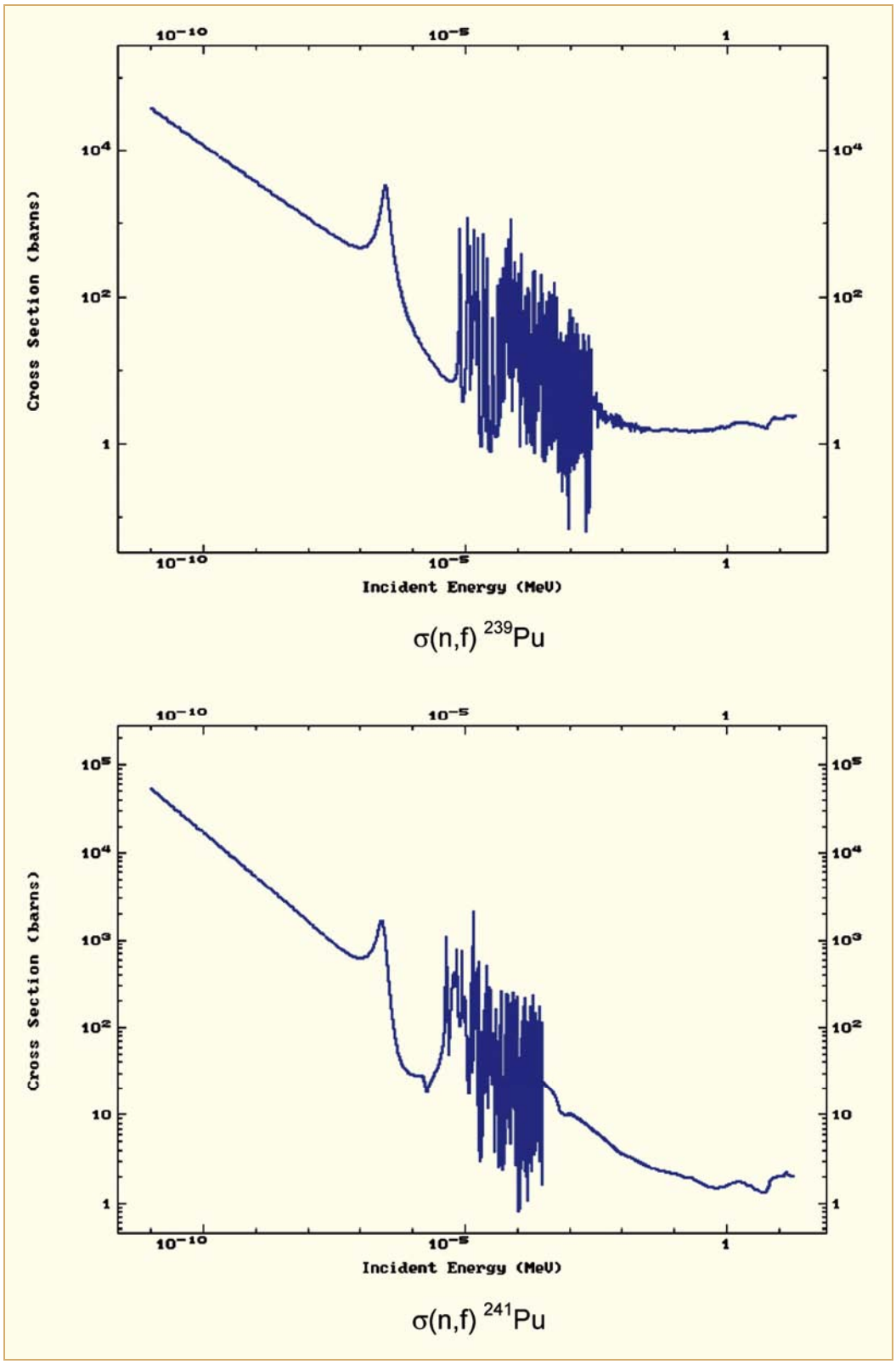

Figure 2-4: Fission cross-sections relative to neutron energy for ^{239}Pu and ^{241}Pu. NB: Note differences in cross-section scales [NNDC, 2010].

Table 2-1: Summary of microscopic cross-sections and neutron yields [Kaye & Laby 2005].

	Elastic Scattering σ(nn)	Inelastic Scattering σ(nn')	Radiative Capture σ(nγ)	Fission σ(nf)	Average neutron yield (ν-bar)
Fissile materials	Average over thermal spectrum (barns)[1]				
^{235}U	15.98		86.70	504.81	2.433
^{239}Pu	7.90		274.32	699.34	2.882
^{241}Pu	12.19		334.11	936.65	2.946
Fertile materials					
^{238}U	9.37		2.41	1.05E-05	2.489
^{240}Pu	1.39		262.65	6.13E-02	2.784
Fissile materials	Slowing-down region resonance integrals (barns)[2]				
^{235}U	152.82		131.97	271.53	2.438
^{239}Pu	155.87		184.06	289.36	2.876
^{241}Pu	148.68		169.13	570.66	2.933
Fertile materials					
^{238}U	319.06		277.70	2.16E-03	2.490
^{240}Pu	913.76		8448.70	3.74	2.785
Fissile materials	Average over fission spectrum (barns)[3]				
^{235}U	4.409	1.917	0.095	1.219	2.583
^{239}Pu	4.566	1.369	0.065	1.800	3.091
^{241}Pu	5.170	1.048	0.226	1.626	3.151
Fertile materials					
^{238}U	4.825	2.598	0.070	0.300	2.598
^{240}Pu	4.996	1.418	0.095	1.349	3.013

Notes
1. The low energy, thermal spectrum ranges from 1E-4 eV to 1.0 eV.
2. At intermediate energies (0.5 eV to 100 keV), cross sections are given by the respective resonance integrals rather than averages.
3. The fission spectrum ranges from 1 keV to 20 MeV with the greatest contribution from a narrow energy band around 2 MeV.

The fission cross-section increases with decreasing neutron energies for the fissile isotopes ^{235}U, ^{239}Pu and ^{241}Pu as shown in Figure 2-3 and Figure 2-4. The energy of fission neutrons decreases due to interactions with moderating material such as the coolant in a Pressurized Water Reactor (PWR) or a Boiling Water Reactor (BWR). This decrease leads to a distribution in which neutron energies are in approximate equilibrium with the energy of the moderator. This energy varies with temperature and gives rise to the thermal spectrum shown in Figure 2-5. Thermalized neutrons are the principal source of fission in water reactors.

3 Fuel chemistry

The oxidation state and the related O/U or Oxygen-to-Metal (O/M) ratios are arguably the most important chemical properties of UO_2 fuel relative to its in-reactor behaviour [Walker et al, 2005]. The oxygen potential of nuclear fuel, $\Delta\bar{G}_{O_2}$ or (more conveniently) $\Delta G(O_2)$, affects the thermal conductivity of the fuel as well as diffusion controlled processes such as grain growth, creep and Fission Gas Release (FGR). It also affects the chemical state and behaviour of FPs and can contribute to the oxidation of the inner surface of zirconium-alloy cladding.

For reference, the oxygen potential of a ceramic (or other solids) is the partial molal free energy of oxygen in the solid per mole of gaseous oxygen. It represents the difference between the chemical potential of oxygen in the solid and the chemical potential of gaseous oxygen at the same temperature and a standard pressure, generally 1 atm. This condition is shown schematically for UO_2 in Figure 3-1.

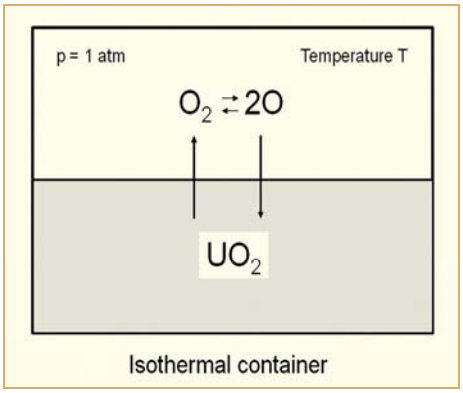

Figure 3-1: Schematic diagram of thermodynamic equilibrium between gaseous oxygen and solid UO_2

The oxygen potential is defined as:

$$\Delta\bar{G}_{O_2} \equiv RT\ln\left(p_{O_2}\right)$$

and is equal to:

$$\Delta\bar{G}_{O_2} = 2\mu_{O_{solution}} - \quad G^{\circ}_{O_2}$$

with

$\mu_{O_{solution}}$ = Chemical potential of oxygen in solution

and

$G^{\circ}_{O_2}$ = Gibbs free energy of gaseous oxygen at temperature T and a standard pressure; e.g., 1 atm.

These relationships are discussed in standard references on thermochemistry; e.g., [Kubaschewski & Alcock, 1983]. Specific applications to UO_2 and $(U,Pu)O_2$ are presented by [Olander, 1976]. The relationships are included here as background for a more general review of fuel properties and performance.

The significant point regarding oxygen potential is that the stability of a ceramic relative to the exchange of oxygen increases as $\Delta\bar{G}^{\circ}_{O_2}$ becomes more negative. For example, the oxygen potential of UO_2 is approximately -750 kJ/mol at 350 °C, while the free energy of formation of ZrO_2 is about -980 kJ/mol at the same temperature. This indicates that oxygen from UO_2 is expected to react with Zr to form ZrO_2 if given sufficient time and a favourable diffusion path. Alternately, oxygen would remain in UO_2 rather than reacting with a FP such as palladium, which has an oxygen potential of approximately -110 kJ/mol at 350 °C. This point is discussed further in text that follows and in a subsequent section on FPs and their chemical state.

The uranium-oxygen (U-O) system includes a relatively large number of chemical states due to the range of valances in which uranium can exist; i.e., U^{3+}, U^{4+}, U^{5+} and U^{6+}. The most stable states are U^{4+}, U^{5+} and U^{6+}, with U^{4+} being the primary valance state of interest in the performance of water reactor fuel. A partial phase diagram of the U-O system is shown in Figure 3-2. This diagram is centred around highly stable, stoichiometric urania ($UO_{2.00}$) and is a composite of information from several sources; viz., [Levin & McMurdie, 1975], [Olander, 1976], [Kim, 2000], [Guéneau et al, 2002], [Baichi et al, 2006] and [Rudling et al, 2007].

For reference, all lattice sites in a stoichiometric ceramic are filled according to the normal chemical formula. Deviations from stoichiometry in UO_2 involve an excess or deficit of oxygen; viz., UO_{2+x} or UO_{2-x}, respectively. A state of non-stoichiometry is commonly expressed as $UO_{2\pm x}$. As indicated in Figure 3-2, the range of non-stoichiometric urania is relatively large.

In Figure 3-2, the “solidus” boundaries identify temperatures at which liquid first appears in the solid phase on heating. Similarly, the “liquidus” boundaries identify temperatures at which solids first appear in the liquid phase on cooling. A region bounded by solidus curves, such as $UO_{2\pm x}$, is solid. The region above the liquidus curve is liquid.

In the typical sintering process used to produce fuel pellets, cooling pure urania in a reducing atmosphere gives an O/U ratio of 2.000 ± 0.001; e.g., cooling from temperatures greater than 900 °C in H_2 [Baichi et al, 2006]. The observed O/U ratios of as-sintered pellets generally vary by a larger amount (±0.005 to ±0.02) due to factors such as impurities or additives in the sintered pellets, variations in the oxygen potential of the atmosphere in which the O/U ratio is set and the measurement process itself. In typical water reactor fuel, UO_2 begins operation as nearly stoichiometric or slightly hyperstoichiometric material. This condition is highly advantageous because it avoids phase transformations at temperatures up to melting and, as is discussed later, minimizes the adverse effects of on non-stoichiometry on defects in the crystal structure and on the resulting thermal and mechanical properties of the fuel.

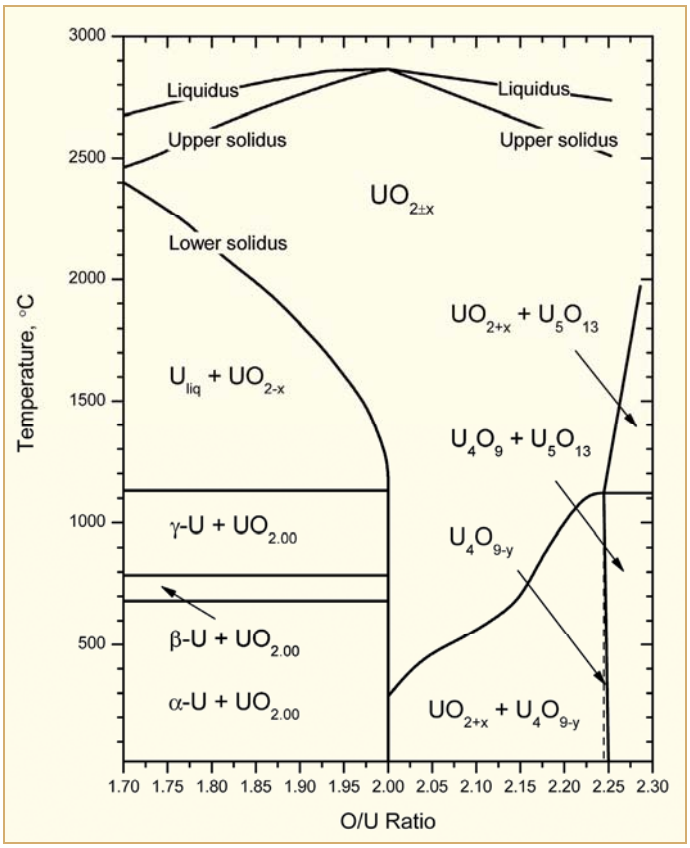

Figure 3-2: Partial phase diagram of the uranium-oxygen system. NB: Vertical lines represent the UO_2 and U_4O_9 compounds.

The plutonium – oxygen system, Pu – O, is similar to the U – O system in that plutonium can also exist in a number of valence states; i.e., Pu^{3+}, Pu^{4+}, Pu^{5+} and Pu^{6+}. The most stable states are Pu^{3+} and Pu^{4+}. The phase diagram for the Pu – O system is shown in Figure 3-3. The region of interest for water reactor fuel centres around the stoichiometric compound PuO_2; i.e., x(O) = 0.67 in Figure 3-3.

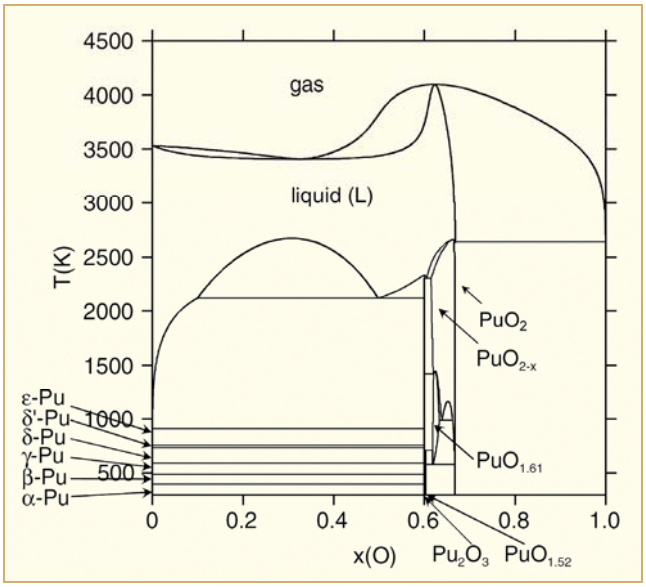

Figure 3-3: Pu – O phase diagram [Guéneau et al, 2008].

4 Crystal structure of UO_2

The crystal structure of UO_2 corresponds to the fluorite lattice shown in Figure 4-1, which derives its name from the compound CaF_2. The oxygen ions (O^{2-}) in the anion sublattice are located in a cubic array, with uranium ions (U^{4+}) occupying half of the available cation sites of the space lattice. The uranium ions in the cation sublattice are located in a face-centred cubic array. Solid solutions with other elements such as plutonium, gadolinium or rare earth FPs involve the replacement of uranium ions with alternate cations in the cation sublattice. In the case of cations with valance other than 4^+, solid solution also involves the formation of point defects.

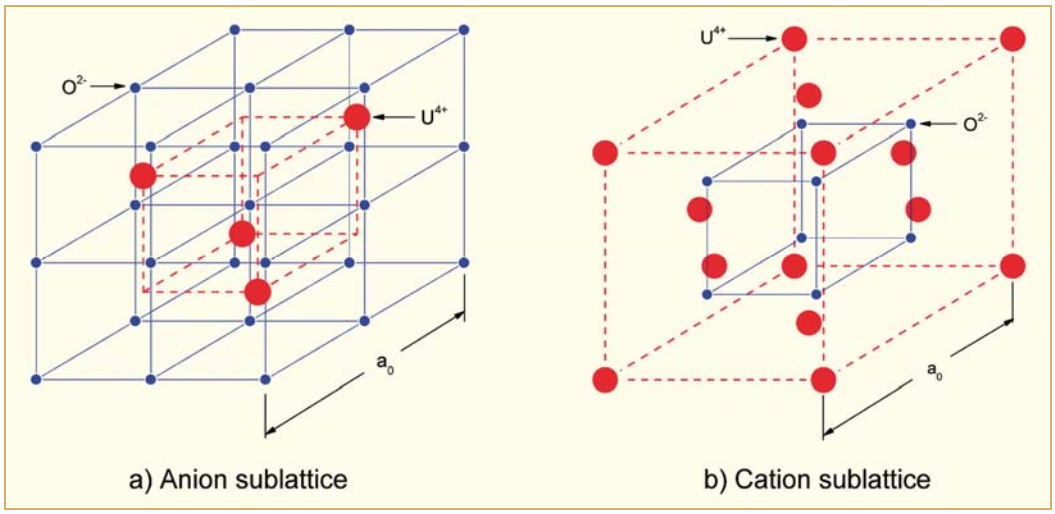

Figure 4-1: Fluorite crystal structure of UO_2 Lattice parameter, a_0 = 5.47 Å, after [Olander, 1976].

As noted in the introductory section, characteristics of the fluorite structure make UO_2 and $(U,Pu)O_2$ well suited for use as a fuel material. One such characteristic is the large number of vacant sites in the fluorite structure. These sites can accommodate FPs with little distortion of the overall lattice, particularly as compared to metallic fuel materials. A second characteristic is the stability of the structure over a wide temperature range; i.e., the basic, fluorite structure remains unchanged at temperatures up to the point of melting. Additional characteristics involve chemical stability relative to cladding and coolant materials and a general tolerance for radiation damage.

Radiation affects the crystalline structure of UO_2 mainly through the interaction of charged, high energy emissions with the ions comprising the fluorite lattice. This is particularly true for fission fragments formed during operation which, as noted in Chapter 2, are massive and highly energetic, i.e., atomic mass numbers in the range of 75 to 160 and initial kinetic energies of 70-100 MeV. This energy is dissipated by collisions with ions in the fuel matrix (and with atoms dispersed among fuel particles) over a cylindrical path that is 7-10 μm in length and 150-200 Å in diameter. Since the energy required to displace an atom from its normal lattice site is approximately 20-40 eV [Olander, 1976], each fission fragment displaces a large number of atoms through direct collisions with lattice ions (identified as primary knock-ons) and through collisions between the affected ions and other lattice ions (identified as higher order knock-ons). The estimate by Olander given in Table 4-1 indicates over 20 000 uranium ions can be affected in the collision-displacement cascade created by each fission fragment. Lattice ions can also be displaced by kinetic and electronic interactions with other high energy emissions from fission and decay. These displacements depend on the nature and energy of the emissions, relative masses and related factors such as displacement cross-sections and energy transfer functions. The net result is that the ions comprising UO_2 typically undergo many thousand displacements during their operating life in a water reactor.

Table 4-1: Estimate of knock-on production by fission fragments in UO_2 [Olander, 1976].

Particle	Number per fission fragment	Mean energy keV	Range Å
Fission fragment	1	80 000	100 000
Primary uranium knock-ons	28	100	220
Higher order uranium knock-ons	21 000	0.2	44

The principal type of structural disorder created by fission and decay in UO_2 is the formation of Frenkel defects on the anion sublattice [Olander, 1976]. Frenkel defects, shown in Figure 4-2, are produced when an ion is displaced from its normal lattice site to an interstitial location, thereby creating a vacancy-interstitial pair. Frenkel pairs are been found to be more prevalent in the anion sublattice than in the cation sublattice through studies based on electron microscopy and XRD. This condition arises because of the mass of the fission fragments relative to those of the anions and cations and the respective atomic properties; e.g., atomic number, mass, collision cross-section and spatial density.

Fission and decay also produce a secondary type of structural disorder in UO_2. This disorder, known as Schottky defects, involves the production of vacancy-interstitial pairs in both the anion and cation sublattices. For reference, Schottky disorder in an ionic solid is shown schematically in Figure 4-2. The number of Schottky defects in UO_2 is significantly smaller than the number of Frenkel defects on the oxygen sublattice, but is large enough for the resulting uranium vacancies to control the creep rate of UO_2.

Vacancies and interstitials are separate constituents of the fluorite lattice which affect the behaviour of UO_2. The concentration of vacancies and interstitials depend strongly on temperature as well as the processes of fission and decay. Vacancy concentration and mobility increases with temperature according to Arrhenius relationships. Self diffusion takes place by movement of oxygen vacancies which result primarily from Frenkel disorder and of uranium vacancies formed by Schottky disorder. Vacancies disappear when they combine with the corresponding interstitials to restore the lattice, with other vacancies form voids or bubbles, with structural defects such as dislocations and with grain boundaries and free surfaces. The process of formation, diffusion and recombination or reaction contribute to a wide range of physical behaviour of significance to in-reactor operation. Examples include heat capacity, densification, gaseous swelling hot pressing, creep and restructuring, including the formation of a sub-grain structure in low temperature regions near the outer surface of high-burnup fuel.

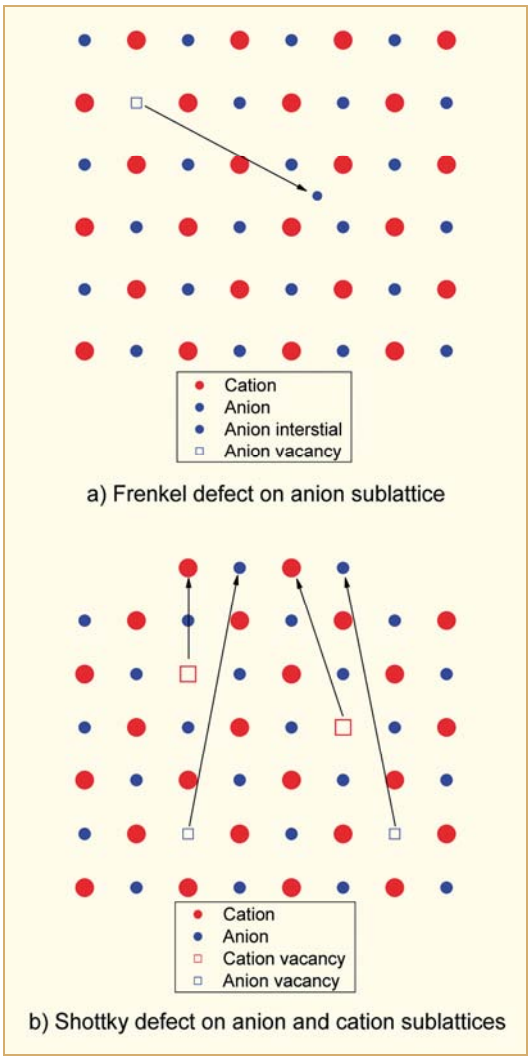

Figure 4-2: Schematic view of Frenkel and Schottky disorder in an ionic solid[6] [Kingery et al, 1976].

The liberation of oxygen by fission discussed in previous sections also affects the crystalline structure of UO_2. Excess oxygen is situated in the vacant cation sub-cells on any of 12 possible <110> directions as shown in Figure 4-3. The ions identified with the number "1" in this figure are the excess, interstitial oxygen. The ions identified with the number "2" are part of the original anion sublattice. These lattice anions are displaced from their normal position by the interstitial ions. For small amounts of excess oxygen, the structure of Figure 4-3 is distributed among a few cells. The valance state of uranium changes from U^{4+} to U^{5+} to maintain electrical neutrality in the affected cells. The valance state of uranium remains at U^{4+} in other cells that do not contain excess oxygen. With increasing excess oxygen, more cells contain the oxygen-defect complex. If the ratio of Oxygen-to-Uranium (O/U) reaches 9:4, the defect complex vanishes and a new phase appears; viz., U_4O_9. This new phase also has the fluorite structure of UO_2 with a unit cell that is four times larger than the original UO_2 cell [Olander, 1976]. This amount of excess oxygen can arise in fabrication, reprocessing or possibly post-failure oxidation of pellets in a leaking fuel rod, but is not expected to occur during normal fuel operation.

[6] Note that Figure 4-2b applies to a "MX" material such as NaCl. In a MX_2 material such as UO_2, a Schottky defect involves one U^{4+} and two O^{2-} ions to maintain electrical neutrality.

5 Fission products

The composition and structure of UO_2 and $(U,Pu)O_2$ changes during irradiation due to the generation of FPs and the manner in which FPs interact with the fuel matrix. That is, about 200 stable or long lived FP atoms are produced fuel per 100 fissions. The cumulative distribution or chain yields of these FPs are shown in Figure 5-1. Their yields vary with neutron energy to a small extent and with the fissioning nuclide to a slightly larger extent.

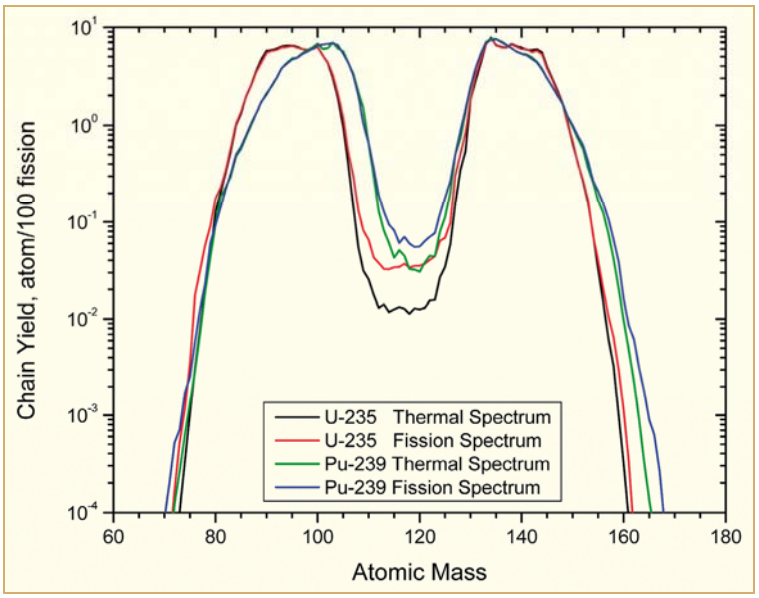

Figure 5-1: Fission yields by atomic mass, fissile isotope and neutron energy [England & Rider, 1994].

An example of the FP inventories in a LWR rod is listed in Table 5-1. These data give the average, net generation rate of each nuclide during operation; i.e., μg of FP per gm of actinide and FP per 10 GWd/MTU. Data in this table are net inventories ≥1 ppm as calculated with the ORIGEN-2.1 computer program with operation at 18.5 kW/m core average power to 60 GWd/MTU. They represent the steady-state FP inventories during in-reactor operation, without loss due to post shut-down decay.

The physical states and chemical forms vary significantly among the FPs. FPs are typically divided into classes based on these forms and on the effects each form has on fuel characteristics and behaviour [Olander, 1976] and [Kleykamp, 1985]. The classes are:

1) Noble gases: The noble gases Kr and Xe, which are essentially insoluble in the fuel matrix and can form either intragranular (within grain) voids of bubbles, intergranular (grain boundary) bubbles or be released from the fuel pellets to the free volume of the respective fuel rod.

2) Volatiles: Elements such as Br, Rb, Te, I and Cs, that exist as gases at high temperatures typical of the interior of an operating fuel pellet or as solids at the cooler exterior of a pellet.

3) Metals: Elements such as Mo, Ru, Pd, and Tc that form metallic precipitates and insoluble metallic alloys.

4) Insoluble oxides: Elements such as Zr, Ba and Sr that form oxides and are insoluble in the fluorite lattice.

5) Soluble oxides: Elements such as Y, La and the rare earths that are soluble in the cation sublattice.

Table 5-1 is structured according to these classifications, with notes regarding multiple states or chemical forms for the affected FPs.

Helium is not strictly a FP and is ignored in the following discussions. Helium is, however, produced during and after irradiation by α-decay of fissile materials and actinides. The contribution of helium released from fuel pellets to the total helium inventory in the free volume of a fuel rod is small; e.g., <1% for typical UO_2 rods and 5-6% for MOX rods [Lanning et al, 2005]. Although the total production of helium during irradiation and storage due to decay is estimated to be four times the production of Kr and Xe due to fission [Ronchi & Hiernaut, 2004], the production rates and release fractions of helium during operation are small enough to have only a minor effect on the behaviour of typical LWR fuel and are neglected in some models of thermal-mechanical performance; e.g., FRAPCON-3 [Lanning et al, 2005]. Helium generation and release are potential issues for extended storage of spent nuclear fuel and possibly for designs that are being considered to burn actinides as part of fuel recycling, but do not appear to be a significant factor in the operation of current LWR fuel and are mentioned only in passing in this STR.

The state and chemical form of the FPs depends strongly on the local temperature and oxygen potential within a fuel pellet. As indicated in Table 5-1, volatile FPs can exist as elemental gases at temperatures above their boiling points or as either elemental solids or compounds at lower temperatures. When the local pellet temperature exceeds the respective vaporization temperature of the volatile FPs, they behave as a gas and contribute to void formation and the gas release process like xenon and krypton. Under such conditions, the volatile FPs also tend to diffuse from high temperature regions near the pellet centreline to lower temperature regions toward the outer pellet surface or to escape from the hot interior and condense in the cooler pellet-cladding gap. It should be noted that at temperatures relevant to LWR fuel rods, iodine is a gas during operation (boiling point = 184 °C) while caesium and cadmium are gases at the interior of fuel pellets when operating at moderate-to-high power (boiling points = 671 and 767 °C, respectively). The physical state of these FPs enable their migration to the pellet-cladding interface, where the zirconium alloy cladding is susceptible to iodine-induced SCC and possibly caesium-assisted liquid metal embrittlement by cadmium [Adamson et al, 2006/2007].

Variations in temperature combined with local oxygen potentials affect the chemical form of the FPs that exist as metals and oxides. The tendency of a FP to form an oxide depends on the local temperature, composition and oxygen potential of the fuel matrix. The effect of temperature on the oxygen potential of some of the prominent FPs is shown in Figure 5-2. In a multi-component system such as irradiated UO_2, the relative oxygen potentials of the components indicate whether a given component will oxidize or remain in an elemental form. For example, the oxygen potentials of FPs such as Zr, Ba, Y and the rare earths are more negative than those of UO_2 (or $(U,Pu)O_2$). This implies or reflects the fact that they have a greater affinity for oxygen than UO_2 and tend to exist as oxides in irradiated UO_2, particularly in the presence of excess fission oxygen. Conversely, the oxygen potentials of FPs such as Pd, Rh, Ru, Te and Tc are less negative than UO_2. These FPs will give up oxygen to UO_2 and exist as metals. Depending on the oxygen potential of the fuel matrix, FPs such as molybdenum can exist as a metallic inclusion at high temperatures or as an oxide at low temperatures[7]. The relatively high rate at which Mo is produced as a FP and its affinity for oxygen is a significant factor in the evolution of the O/M-ratio of fuel during operation. This topic is discussed in greater detail in Chapter 3. Caesium is another FP which can exist as a metal or an oxide. Based on its chemical activity and the availability of other reactive FPs, however, caesium can also form alternate compounds such as CsI or Cs_2UO_4.

[7] The partitioning of molybdenum between the oxide and elemental forms is sometimes used as an indicator of fuel temperature during hot cell examinations. This method is most applicable to high power fuel where high centerline temperatures, steep thermal gradients and extensive grain growth leads to the agglomeration of metallic FPs in large (observable) nuggets. It is also most applicable in low exposure fuel where the confounding effects of changing O/M-ratio are small. The partitioning of Mo tends not to be as effective in fuel typical of commercial LWRs, however, due to lower operating powers and higher exposures.

As noted in Chapter 3, soluble FPs affect the oxidation state of the uranium and plutonium comprising the cation lattice. Changes in the oxidation state of uranium are necessary because, as shown in Table 5-1, the valance state of most soluble FPs is 3^+. The incorporation of these ions into the cation sublattice requires the oxidation of sufficient uranium in the region of the soluble FP from U^{4+} to U^{5+} or U^{6+} to maintain electrical neutrality. This condition alters the O/M ratio and affects the chemical state of the FPs that shift between metals and oxides. The effect of soluble FPs on the oxidation state is further confounded by the presence of plutonium, which can exist as Pu^{3+}, Pu^{4+}, Pu^{5+} and Pu^{6+}. As noted earlier, the addition of soluble FPs and the oxidation of uranium to higher valance states generally leads to the reduction of plutonium from Pu^{4+} to Pu^{3+}. The net effect of the soluble FPs is to change the composition and fundamental size of the fuel structure.

FPs are significant to in-reactor and post-irradiation behaviour because of their effects on fuel properties. The FPs krypton and xenon are produced at a combined rate of approximately 168 wt. ppm per GWd/MTU, Table 5-1, which corresponds to 29.2 l/GWd Standard Temperature and Pressure (STP). This gas contributes to FP swelling of the fuel pellets, degradation of thermal conductivity of the pellets, degradation of the thermal conductance of the pellet-cladding gap and to increased pressure inside of fuel rods. Although this STR focuses primarily on thermal and mechanical behaviour, it should be noted that the production, transmutation and decay of ^{135}Xe also affects the nuclear behaviour of the fuel and the reactor core because of its large production rate (6.54 atoms per 100 fissions of ^{235}U)and large neutron absorption cross-section (σ_a = 2.65E6 barns for thermal neutrons) and moderate half life (9.10 hr). Overall, FPs are produced at a rate of ~1% per GWd/MTU, Table 5-1. As with the noble gases, the increase in FP concentration affects a number of fuel properties during operation. Such changes are discussed on a topical basis in the sections which follow.

6 Thermal properties

6.1 Melting temperature

The avoidance of melting in UO_2 and MOX pellets is typically a critical safety criterion for water reactor fuel in most licensing and operating arenas. That is, fuel must be designed and operated so that the peak centreline temperatures remain below the melting point during normal operation and during anticipated operating occurrences that lead to temperatures greater than normal. As noted in an earlier section, the solidus temperature is the lowest temperature at which liquid remains on cooling and is generally taken as the temperature for the onset of melting in fuel design and operation.

The solidus and liquidus temperatures of UO_2 and $(U,Pu)O_2$ have been measured by several techniques; e.g., V-filament heating, thermal arrest and direct laser heating. As shown in Figure 6-1, considerable scatter exists among the measurements. This scatter is due, in part, to the tendency of UO_2 to pick up oxygen, vaporize or react with its containment structure at high temperatures. As a result, data from thermal arrest measurements, where samples are sealed in refractory metal (tungsten) containers, tend to constitute the principal source for solidus and liquidus temperatures.

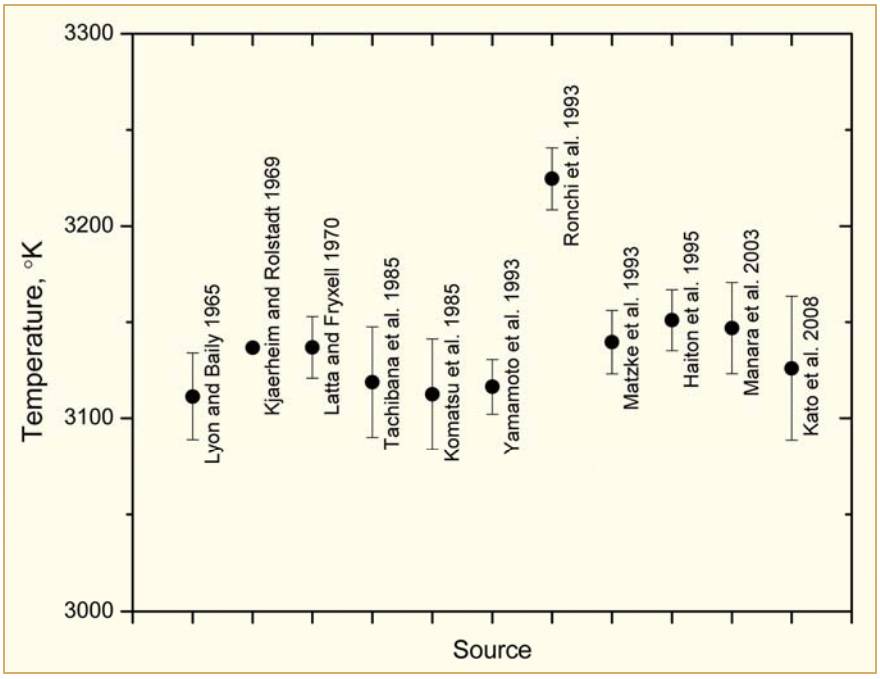

Figure 6-1: Comparison of $UO_{2.00}$ melting temperature from historic sources, after [Kato et al, 2008].

The available data have been compiled and evaluated to address the effects of differences in the experimental methods and to arrive at recommended values. Examples of these evaluations are the joint study by the Russian Research Centre "Kurchatov Institute" and the Oak Ridge National Laboratory [Popov et al, 2000], and the studies by the [IAEA, 2006] and the [INSC, 2010]. The solidus and liquidus temperatures recommended by the Kurchatov Institute and Oak Ridge National Laboratories (ORNL) are [Popov et al, 2000].

$$T_m(UO_{2.00}) = 3120 \pm 30 \text{ K},$$

$$T_m(PuO_{2.00}) = 2701 \pm 35 \text{ K}.$$

From the same source, the effects of varying mixtures of UO_2 and PuO_2 and of burnup are given by:

(Eq. 6-1) $$T_L(y) = 3120.0 - 388.1y - 30.4y^2$$

and

(Eq. 6-2) $$T_S(y) = 3120.0 - 655.3y + 336.4y^2 - 99.9y^3 - 0.5B$$

where

T_L = Liquidus temperature, K,
T_S = Solidus temperature, K
y = Mole fraction of PuO_2,
B = Burnup, GWd/MTU.

For low concentrations of plutonia, the estimated, two-standard-deviation uncertainties are ±55 K and ±35 K for the liquidus and solidus temperatures, respectively. The liquidus and solidus temperatures in the unirradiated state from these relationships are shown in Figure 6-2 for varying concentrations of PuO_2 in UO_2. The solidus from the computer program FRAPCON-3 is included for reference [Lanning et al, 2005]. Solidus temperatures over a range of exposures for UO_2 and $(U,Pu)O_2$ typical of LWR fuel are shown in Figure 6-3. The solidus temperatures from FRAPCON-3 are the same as those shown in this figure. Note that Popov and co-workers do not provide a burnup correction for the liquidus temperature. *The liquidus correction is assumed to be the same as the solidus correction based on the MATPRO relationships [Hagrman (ed.), 1993], but is omitted for consistency with the published document.* Note also that neither the IAEA nor the INSC recommendations include a correction for exposure. These recommendations use the solidus given by Popov and are nearly identical to each other. The rational for this position is less than clear but seems to be based on assessments that the decrease in solidus temperature with burnup is small. *From a pragmatic viewpoint, the positions of the IAEA and INSC seem valid. That is, the thermal margin to the onset of pellet melting tends to affect fuel design and operation at exposures below ~30 GWd/MTU, when fuel reactivity is still high and the magnitude of the temperature reduction is small; i.e., ≤15 °K versus ±30 °K uncertainty. Nevertheless, computer codes intended for the analysis of thermal-mechanical conditions in high burnup fuel rods typically include an exposure-based melting model; e.g., FRAPCON-3 [Lanning et al, 2005].*

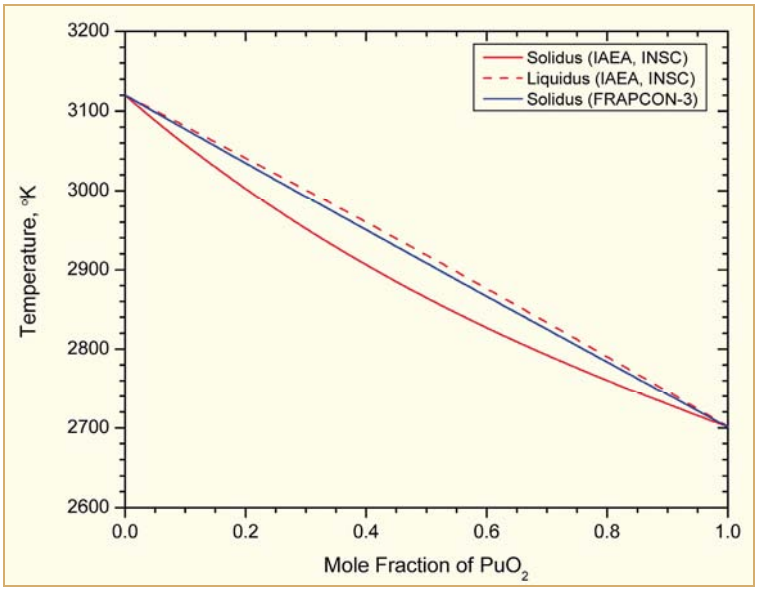

Figure 6-2: Solidus and liquidus temperatures of UO_2 and PuO_2 at beginning of life, based on [Popov et al, 2000] and [Lanning et al, 1997].

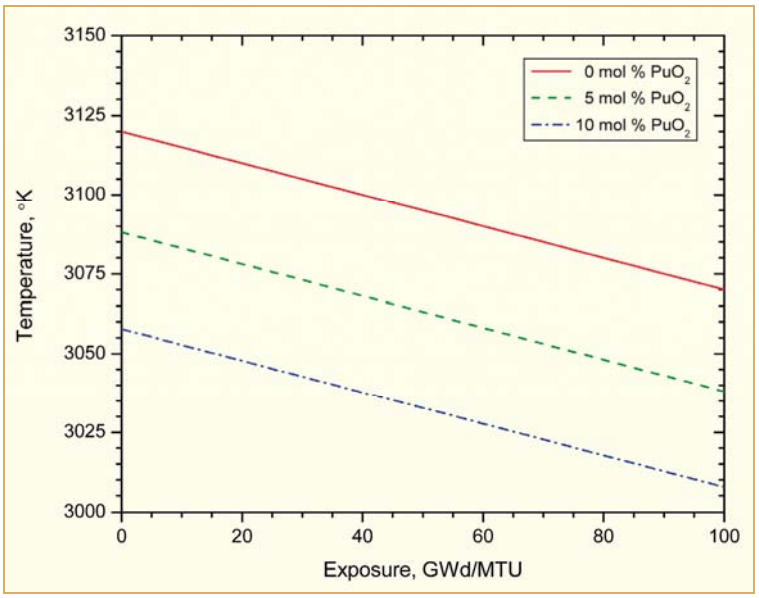

Figure 6-3: Solidus temperature of UO_2 and $(U,Pu)_2$ relative to exposure, based on [Popov et al, 2000].

From the discussion of fuel chemistry in Chapter 3, the solidus and liquidus temperatures of UO_2 and PuO_2 clearly depend on the O/M-ratio. Relationships for melting do not typically address the O/M-ratio, however, because it remains close to the stoichiometric value where variations in the O/M-ratio have only a small effect on the melting temperature. Based on the information presented in Chapter 3, the O/M-ratio at the interior of an operating fuel pellet is expected to range from about 1.995-2.005. From the evaluation of the hyperstoichiometric region by [Manara et al, 2003], summarized in Figure 6-4, the effect of a variation in O/M-ratio from 2.000 to 2.005 is within the uncertainty in the solidus data; i.e., ~20 K decrease vs. ±30 °C uncertainty.

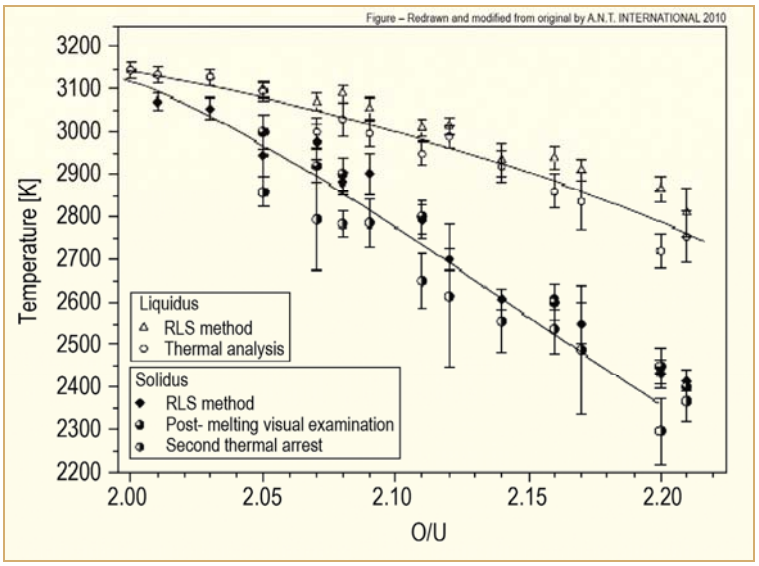

Figure 6-4: Solidus and liquidus temperatures of UO_2 relative to O/U-ratio, after [Manara et al, 2005].

7 Physical properties

7.1 Density

The density of fuel pellets depends on factors such as composition, porosity, temperature and burnup. The theoretical densities of solid, stoichiometric UO_2 and PuO_2 are listed in Table 7-1. The value recommended by the IAEA and INSC for stoichiometric UO_2 is 10.963 gm/cm^3 at 273 K.

Table 7-1: Summary of recommended UO_2 and PuO_2 densities.

Source	UO_2		PuO_2	
	ρ_{TD} gm/cc	T_{ref} °K	ρ_{TD} gm/cc	T_{ref} °K
ANL[9]	10.970	298		
NFD[10]	10.960	298		
Harwell[11]	10.970	273		
ORNL-RRC[12]	10.970	273	11.460	273
IAEA[13]	10.963	273		

The T.D. of $(U,Gd)O_2$ fuel is given by:

(Eq. 7-1) $$\rho_{TD}\left((U,Gd)O_2\right) = 10.960 - 0.031g$$

where g is the concentration of gadolinia in wt.% Gd_2O_3 and density is in gm/cm^3 [Une, 1986].

The T.D. of MOX fuel can be computed from the densities of UO_2 and PuO_2 based on the mole fraction, y, in $U_{(1-y)}Pu_yO_2$ [Popov et al, 2000]; viz.:

(Eq. 7-2) $$\rho_{TD}(MOX) = (1-y)\rho_{TD}(UO_2) + y\rho_{TD}(PuO_2),$$

which corresponds to

(Eq. 7-3) $$\rho_{TD}(MOX) = \rho_{TD}(UO_2) - 0.490y$$

for the densities in Table 7-1.

[9] Argonne National Laboratory [ANL, 1976]
[10] Nippon Nuclear Fuel Development Company [Une, 1986]
[11] Harwell Laboratory [Harding et al. 1989]
[12] Oak Ridge National Laboratory – Russian Research Center "Kurchatov Institute" [Popov et al, 2000]
[13] International Atomic Energy Agency [IAEA, 2006]

The T.D. of UO_2, $(U,Gd)O_2$ and MOX varies with temperature due to thermal expansion and changes in the lattice parameter. These variations are given by:

(Eq. 7-4)
$$\rho_{TD}(T) = \rho_{TD}(273)\left(\frac{L(273)}{L(T)}\right)^3$$

where *L(273)* and *L(T)* are the respective dimensions at 273 K and the temperature of interest as given in Section 6.3. For reference, the effect of temperature on the theoretical densities of UO_2, $(U,Gd)O_2$ and MOX are shown in Figure 7-1, Figure 7-2 and Figure 7-3. The T.D. decreases non-linearly with increasing temperature from room temperature to the melting point. Density increases slightly with the addition of plutonia in MOX and decreases by larger amounts with the addition of gadolinia in $(U,Gd)O_2$.

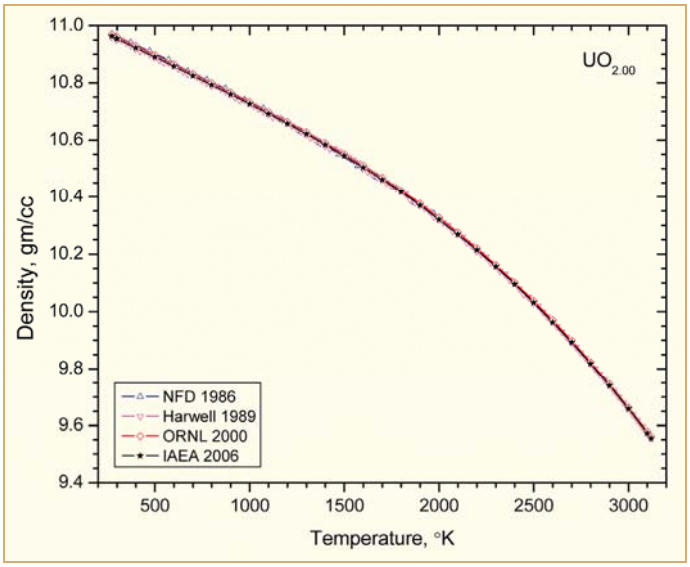

Figure 7-1: T.D. of UO_2 relative to temperature, from equations of [Une 1986], [Harding et al, 1989], [Popov et al, 2000] and [IAEA, 2006].

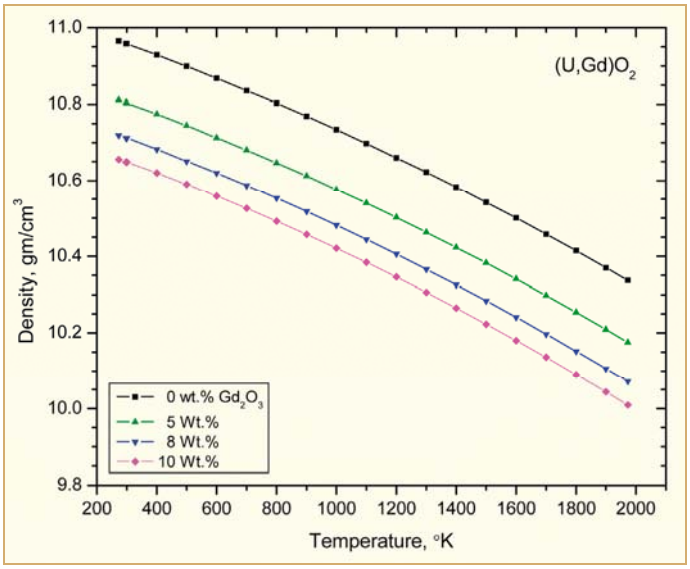

Figure 7-2 : T.D. of $(U,Gd)O_2$ relative to temperature and Gd_2O_3 concentration, from equations of [Une, 1986].

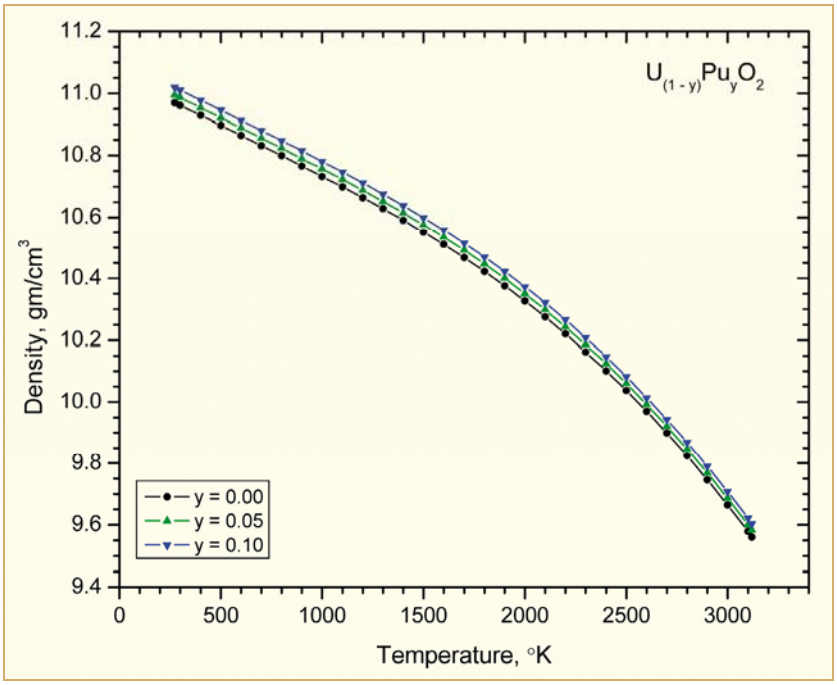

Figure 7-3: T.D. of MOX relative to temperature and plutonium concentration, from equations of [Popov et al, 2000].

Based on the review and recommendations by [Martin, 1988], the linear thermal expansion of UO_{2+x} appears to be insensitive to stoichiometry deviations in the operating range of typical fuel; i.e., x = 0-0.13. In the absence of equivalent data on $(U,Gd)O_2$ and MOX, these materials are assumed to behave in a similar manner [IAEA, 2006]. As a result, the preceding equations are believed to approximate in-reactor conditions without adjustment for stoichiometry.

LWR fuel is fabricated with initial densities in the range of 94-98% T.D. Actual densities are lower than the theoretical values because of porosity that remains from the sintering process and, commonly, that is formed deliberately during fabrication by the use of pore forming materials. Porosity, p, is related to density according to:

(Eq. 7-5) $$p = \frac{\rho_{TD} - \rho}{\rho_{TD}}.$$

The as-built pellet density increases during the initial 5-15 GWd/MTU of operation due to the process of densification. Density increases during this interval because of the closure of small pores due to the combined effects fission fragments, surface energy and diffusion. As noted in Chapter 5, the accumulation of FPs causes fuel density to decrease. Solid FPs lead to lattice dilation that decreases density. The formation and growth of fission gas bubbles further decreases pellet density. The increase in volume that comes from decreasing density can be mitigated somewhat by reductions in pore and bubble volume by hydrostatic stress and hot pressing. In general, density reaches a maximum during the initial 5-15 GWd/MTU interval and then decreases with continued operation. This combination of processes is discussed in subsequent sections dealing with in-reactor behaviour.

7.2 Elastic moduli

The elastic moduli of fuel material are among the fundamental factors in the mechanical behaviour of fuel rods; they determine the effective stiffness of fuel pellets during a rapid power increase and affect the ability of fuel pellets to strain their cladding during a ramp with firm pellet-to-cladding mechanical interaction. The elastic moduli are determined by loading experiments such as axial compression of cylindrical pellets and the flexural or torsional bending of bars and by resonant frequency techniques [ASTM, 2009]. The moduli vary with temperature, density, O/M-ratio and composition [Hagrman, 1993]. Data indicate the elastic moduli increase slightly with PuO_2 concentration in MOX fuel independent of O/M-ratio. Limited data also indicate Young's modulus increases by a larger extent with the concentration of Gd_2O_3 in $(U,Gd)O_2$ fuel [Bibilashvili et al, 2003].

The fluorite lattice and the resulting polycrystalline fuel pellets exhibit isotropic deformation under mechanical loading, so the elastic behaviour is represented two parameters, Young's modulus (E) and the shear modulus (G) or Poisson's ratio (ν). These parameters are independent of direction within the material. The relationship given in the MATPRO set of equations [Hagrman, 1993] and used in the FRAPCON-3 code are:

(Eq. 7-6) $$E_{2.00} = 2.334\times10^{11}\left[1-2.752\left(1-\rho_{ftd}\right)\right]\left(1-1.0915\times10^{-4}T\right)$$

and

(Eq. 7-7) $$E = \left(1+0.15f\right)\exp\left(-b|x|\right)E_{2.00}$$

in which

$E_{2.00}$ = Elastic modulus of stoichiometric UO_2, Pa,

E = Elastic modulus for non-stoichiometric UO_2 or MOX, Pa,

T = Temperature, K,

b = 1.34 for O/M < 2.00 or 1.75 for O/M > 2.00,

f = PuO_2 concentration, wt. fraction,

x = Deviation from stoichiometry; i.e., 2.00 – O/M ratio

and

ρ_{ftd} = Density as a fraction of the theoretical value.

The estimated standard error for stoichiometric UO_2 in Pa is:

(Eq. 7-8) $$\sigma = \begin{cases} 6\times10^{9} & \text{for } T \le 1600^{\circ}K \\ 6\times10^{9}+\left(\dfrac{T-1600}{6052.6}\right)E_{2.00} & \text{for } T > 1600^{\circ}K \end{cases}, \text{Pa}.$$

The estimated standard error for non-stoichiometric or MOX fuel is:

(Eq. 7-9) $$\sigma = \sqrt{\sigma^2+\left(E-E_{2.00}\right)^2}, \text{Pa}.$$

The shear modulus is related to Young's modulus according to:

(Eq. 7-10) $$G = \frac{E}{2\left(1+\nu\right)}$$

in which ν is Poisson's ratio as given in the next section.

8 In-reactor behaviour

8.1 Pellet temperature

The heat generated by fission increases the temperature of the fuel pellet which, in turn, causes heat to flow from the pellet to the coolant. For steady-state operation or transients in which the rate of power change is sufficiently slow that the effects of heat capacity can be neglected, heat generation and temperature are related according to the standard equation for cylindrical coordinates:

(Eq. 8-1) $$\frac{1}{r}\frac{d}{dr}\left(\lambda\, r \frac{dr}{dT}\right) + Q = 0$$

with

- r = Radial position within the fuel pellet,
- Q = Heat generation per unit volume,
- λ = Thermal conductivity

and boundary conditions

(Eq. 8-2) $$T\left(r_{outer}\right) = T_{surface}$$

and

(Eq. 8-3) $$\left(\frac{dT}{dr}\right)_{center} = 0\ .$$

As discussed in Chapter 2, heat generation (q) varies across the pellet radius due to the depression of fission rate by neutron self-shielding and due to fuel-related changes during operation; e.g., the conversion of ^{238}U to ^{239}Pu and the generation of high cross-section FPs. Similarly, thermal conductivity also varies across the pellet radius due to the factors discussed in Section 6.5; e.g., temperature, burnup, porosity, O/M-ratio and radiation damage. As a result, equation (Eq. 8-1) is highly non-linear and is usually solved incrementally using numerical methods. Do not despair, however; the objective of this section is the effect of in-reactor operation on fuel temperature and not the numerical methods needed to evaluate fuel temperature.

The distribution of temperature across the radius of a typical LWR fuel rod is shown in Figure 8-1. In this example, temperature is plotted relative to radial position for a LHGR typical of the upper range of current LWR fuel (40 kW/m) and for a rate typical of the average over the life of BWR or PWR fuel (20 kW/m). Temperatures in this plot are based on a Zircaloy-clad, UO_2 rod at the beginning of irradiation. The surface temperature of the fuel pellet (boundary condition (Eq. 8-2)) is fixed by the bulk coolant temperature, heat flux and the dimensions and thermal conductivities of the surface film, cladding and the gap (interface) between pellets and cladding. Temperatures in the pellet are given by numerical solution of (Eq. 8-1) starting with the surface temperature.

The noteworthy points in Figure 8-1 are the high temperatures in the pellet interior, the large variations in fuel temperature across the pellet radius and the strong dependence of both pellet temperature and thermal gradients on power. At high LHGRs, temperatures at the pellet interior are great enough to activate thermally driven processes; e.g., creep, FGR (covered in a later section) and other diffusion-based behaviour. Temperatures at the pellet exterior remain below the thermally activated range, which is generally 1200-1300 °C, so that behaviour depends on the athermal, fission-induced processes. The thermal gradients at mid-radius are 90-160 °C /mm for the conditions of Figure 8-1, which leads to thermal stresses in the fuel pellet that exceed its fracture strength. For a given heat generation rate, pellet temperatures increase with burnup due to the growth of Chalk River Unidentified Deposits (CRUD) and oxide at the outer cladding surface, degradation of the gap conductance due to the generation and release of fission gases (Kr and Xe) and degradation of the thermal conductivity of the fuel itself. The temperatures experienced by fuel pellets while in-reactor vary with power and operating history. Power is typically constrained in the design and licensing processes to prevent centre-line temperatures from reaching the melting point when uncertainties and potential over-power conditions are factored into the calculations [Rudling & Patterson, 2009].

An important distinction between the thermal history of BWR fuel relative to PWR fuel arises from the periodic movement of control blades in BWRs. Power is depressed in fuel that is shadowed by a control blade and is higher in the uncontrolled fuel beyond the end of a blade. Power in the uncontrolled region decreases with axial distance above a control blade due to neutron leakage and fewer thermal neutrons from increasing steam (void) fractions. Blades are moved axially during operation to distribute power generation and burnup as uniformly as possible over the length of a each fuel assembly. As a result, the peak power region above a control blade sweeps along the length of each fuel column multiple times over the life of a fuel assembly and causes the peak temperature in early and mid-life to exceed the threshold for thermally-activated processes. Although control rods are also used in PWRs for power shaping, the distribution of power and pellet temperature is typically more uniform along the length of PWR fuel columns due to the use of boron in the coolant for reactivity control. The absence of the sweeping power peak from control blade moves can give lower temperatures and FGR fractions in PWRs than BWRs even though the lifetime-average powers are generally similar.

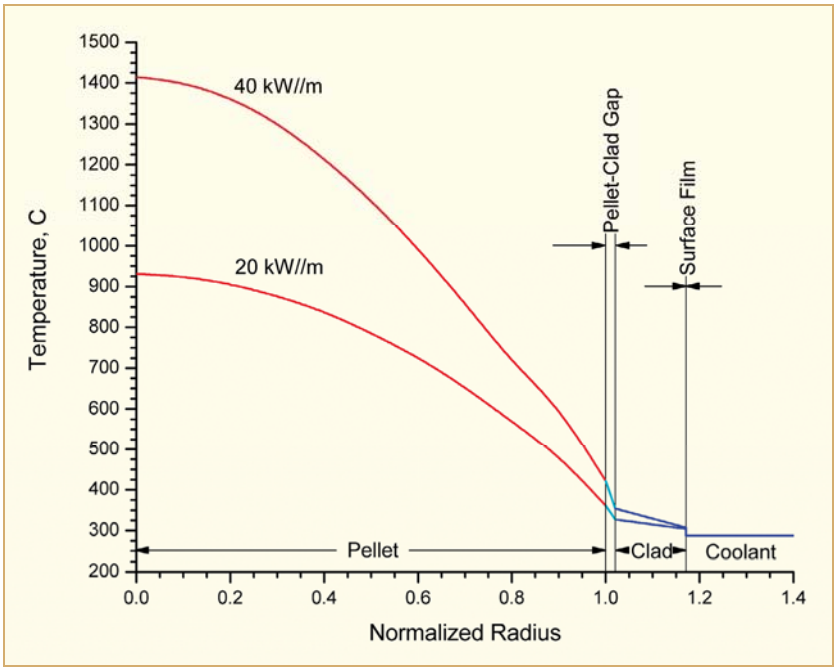

Figure 8-1: Temperature relative to radial position and power in a Zircaloy clad UO_2 fuel rod, from MATPRO equations [Hagrman, 1993].

8.2 Pellet cracking and relocation

Thermal gradients within a fuel pellet give rise to thermal stresses sufficient to fracture a fuel pellet starting on the first rise to power. Higher temperatures near the centreline of an operating pellet causes the fuel in this region to expand more than fuel at the cooler exterior. These thermal strains cause the diameter of a pellet to expand, its ends to dome outward and its overall shape to change from a right, circular cylinder to that of a hourglass or wheat sheaf as shown in Figure 8-2.

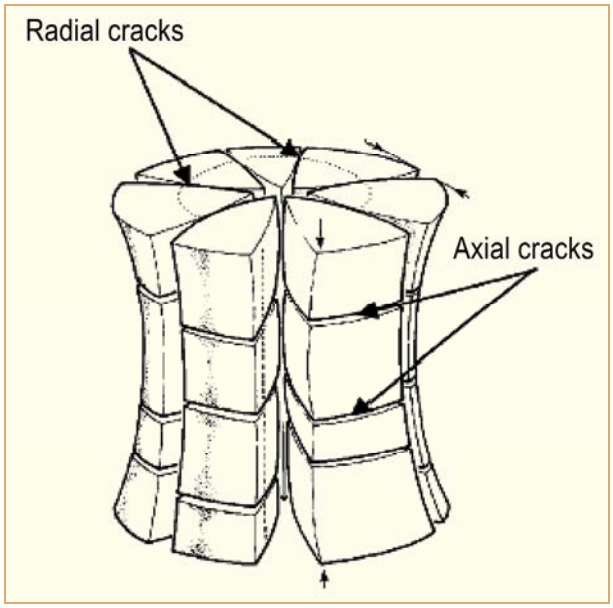

Figure 8-2: Schematic diagram of pellet fragmentation due to thermal stress.

The thermal stress in a fuel pellet is given approximately by:

(Eq. 8-4)
$$\sigma_\theta^{\max} \simeq \frac{\alpha E q}{8\,\pi(1-\nu)\,\bar{\lambda}}$$

where

$\sigma_\theta^{\max}$ = Maximum stress in the circumferential (hoop) direction, MPa,

E = Elastic modulus, MPa,

q = Power, W/m,

α = Coefficient of thermal expansion, 1/ K,

ν = Poisson's ratio

and

$\bar{\lambda}$ = Average thermal conductivity, W/(m K).

The fracture strength of oxide fuel was discussed in Section 7.4 and is approximately 120 MPa at the outer edge of a pellet (cf. Figure 7-9). As a result, pellet cracking begins at about 5 kW/m on the initial rise to power. Cracking is observed to continue with increasing power and exposure through the initial 5-10 GWd/MTU of operation and to progress toward the approximate configuration shown in Figure 8-2.

The understanding of pellet cracking has evolved over time. Initially, pellets were believed to fracture in the brittle outer region but remain in-tact in the ductile interior. With this understanding, the structural behaviour of a pellet is controlled by a combination of forces and displacements in the semi-ductile region between the inner core and outer shell, which can support shear as well as normal loading, and the ductile interior, which can support only hydrostatic loads (see, for example [Olander, 1976]). More significantly, a pellet is predicted with these assumptions to behave as a cracked, but integral entity with respect to heat transfer and pellet-cladding mechanical interaction. In-reactor measurements of fuel elongation and diametral deformation in the Halden Reactor starting in the mid-1970s have shown, however, that mechanical interaction begins at powers well below that required for closure of the current pellet-cladding gap by the differential thermal expansion of pellets and cladding. This interaction was ultimately determined to result from:

- The stochastic radial alignment of fuel pellets relative to their cladding,
- pellet cracking across the full pellet radius and transverse cross-section by means of a dynamic process involving the release of stored energy,
- the misalignment of the resulting pellet fragments,
- the radial movement (relocation) of the pellet fragments relative to the inner cladding surface and
- contact among asperities of adjacent fragments with varying amounts of strength due to frictional forces and due to sintering at the contact asperities with sufficient temperature, pressure and time.

An example of a recent assessment of dynamic fracture is shown in Figure 8-3. This assessment predicts cracks to extend across the full pellet radius in vertical planes and across the full pellet diameter in a horizontal plane located at mid-length. The number of radial cracks is calculated to increases with power. Circumferential cracks are also calculated to form during ramps to higher powers. The results of dynamic fracture mechanics are generally consistent with post-irradiation observations of pellet cracking; i.e., the calculated cracking pattern is similar to the post-irradiation patterns, but does not reflect the variability among actual cracking patterns. Dynamic fracture and the creation of independent fuel fragments are, however, consistent with in-reactor and post-irradiation observations of pellet temperatures and cladding deformation.

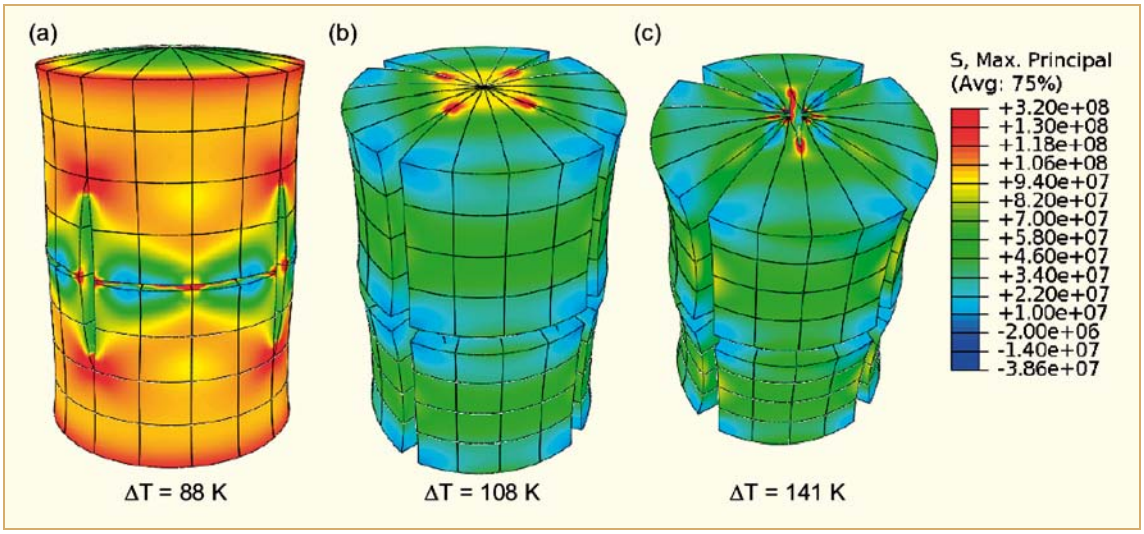

Figure 8-3: Predicted stresses and displacements on initial rise to power due to dynamic fracture, with displacements magnified by 200X for clarity [Williams & Knoll, 2009].

9 Improved pellet materials

Fuel that contains additives, which are also known as dopants, is being developed as a means for improving in-reactor performance and is in varying stages of commercialization. This topic was reviewed in detail by Davies and Vaidyanathan [Adamson et al, 2006/2007]. The significant points from the previous review are presented in this section along with information that has become available since the report by Davies and Vaidyanathan.

The additives of interest fall into two general categories. The first category involves materials that are essentially insoluble in the fluorite lattice and exists as a separate, grain boundary phase; e.g., mixtures of alumina and silica (aluminosilicates or Al-Si-O). The second category involves materials that are soluble in the cation sub-lattice, such as chromia, or involve a mixture of soluble and insoluble materials, such as chromia and alumina. Although many other additives fall into both categories, attention is directed to the aluminosilicate additives and chromia-base dopants as they appear to be the closest to large-scale application.

9.1 Aluminosilicate additives

The first type of additive was developed with the objective of preventing cladding failures due to FP-induced, stress-corrosion cracking; i.e., the PCI failure mechanism. Early work in this area involved materials that form an amorphous, grain boundary phase to reduce yield strength and promote grain boundary sliding [Hill et al, 1972]. Parallel investigations involved optimizations of the additive to improve the ability of the grain boundary phase to alter the chemical state or the release rate of potentially damaging FPs to the inner cladding surface [Grossman et al, 1974]. The aluminosilicate additives were also found to act as a sintering aid which promotes grain growth during pellet fabrication and are receiving additional attention as a means for reducing FGR at high burnup.

Aluminosilicate additives consist of a mixture of SiO_2 and Al_2O_3 that is to blended with UO_2 or UO_2 + Gd_2O_3 powder prior to pressing and sintering. Naturally occurring clay minerals were used in early tests and irradiation programs; viz., bentonite and kaolinite [Davies et al, 1999]. The ratio of SiO_2 to Al_2O_3 is ~82%:18% in bentonite and ~55%:45% in kaolinite. Synthetic blends have replaced the natural minerals to eliminate impurities and to allow adjustment of the SiO_2-to-Al_2O_3 ratio [Hirai et al, 1997]. The synthetic mineral ratio continues to be close to that of kaolinite [Matsunaga et al, 2009].

During the sintering process, the additive forms a glassy phase that collects on the grain boundaries. An example of the resulting microstructure is shown in Figure 9-1. The SEM image in the upper-left quadrant shows the overall structure of an unirradiated UO_2 fuel pellet which contains 2500 ppm of an Al-Si-O additive. The other 3 quadrants of this figure are images from Energy Dispersive Spectroscopy (EDS) which show the presence of the additive on grain boundaries. The additive is believed to cover all grain boundaries with concentrations at the intersection among grains (triple points) and the excess above the basic grain boundary thickness distributed among triple points and grain faces. The additive phase is primarily amorphous but contains isolated crystalline structures as shown in the TEM and Focused Ion Beam (FIB) images of Figure 9-2. EDS analyses indicate the amorphous phase is primarily SiO_2 while the crystalline phase is mullite [Matsunaga et al, 2009].

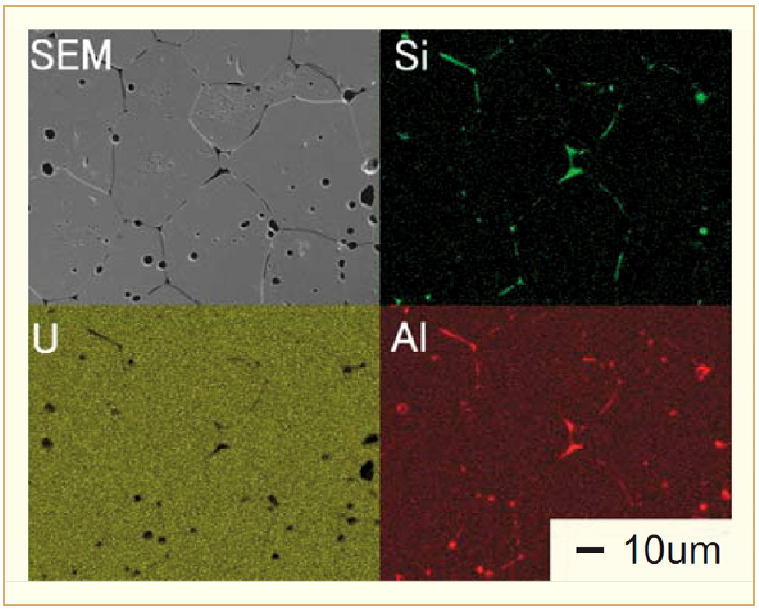

Figure 9-1: Structure of a UO_2 pellet with 2500 ppm Al-Si-O additive as given by SEM and EDS [Matsunaga et al, 2009].

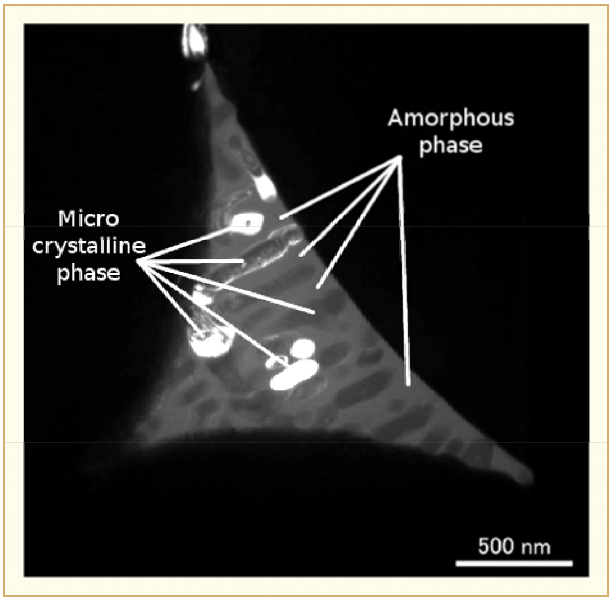

Figure 9-2: Structure of Al-Si-O phase as given by TEM and FIB images [Matsunaga et al, 2009].

While at sintering temperatures, the additive is in a fluid state and promotes grain growth through liquid-phase sintering. The size of the resulting UO_2 grains is in the range of 20-60 μm, depending on the additive concentration and sintering process. The size of $(U,Gd)O_2$ grains in fuel that contains the Al-Si-O additive varies with the Gd_2O_3 concentration but is in the range of additive-UO_2 pellets; e.g., 30-40 μm with 10 wt.% Gd_2O_3 and the Al-Si-O additive versus 5 μm without the additive [Hirai et al, 1997]. The density of sintered additive pellets is typically in the range of 96-98% T.D., with little or no densification in standard re-sintering tests. Note that the density of the additive itself is about one-fourth that of UO_2 after sintering. Consequently, the additive displaces fissile material and is used in low concentrations.

Note also that Al-Si-O additives form a low temperature eutectic with UO_2, Davies and Vaidyanathan in [Adamson et al, 2006/2007]. Regions of fuel above the eutectic temperature will exist in both the solid and liquid phases. Such regions are confined to the hot interior of fuel pellets while at high power and are of limited extent because of the small concentrations of additive. This liquid phase has been observed to relocate from the centre of a fuel pellet to about mid-radius in ramp tests. Post-irradiation examinations show FPs such as caesium also move with the additive and concentrate in the relocated zone. As demonstrated in re-ramp experiments, the resistance of Al-Si-O additives to the PCI failure process does not appear to be affected by relocation of the additive phase. The low temperature eutectic and possible relocation of Al-Si-O additive that is above the eutectic temperature do not seem to affect in-reactor performance, but are issues for design and licensing.

The development of aluminosilicate additives began in the mid-1970's and has involved a wide range of experimental programs [Davies et al, 1999] and [Matsunaga et al, 2009]. Laboratory tests of unirradiated samples were performed to characterize the creep behaviour and strength of additive fuel and to define its thermophysical properties. These tests showed significant increases in the rate of thermal creep, Figure 9-3, and reductions of yield strength of fuel with the Al-Si-O additive, Figure 9-4. This work also showed other thermophysical properties of the additive fuel to be very close to those of non-doped fuel as illustrated in the comparison of thermal conductivities in Figure 9-5. Information on the release of fission gas from additive fuel was presented in Section 8.7 and indicates that the reduction in release rates associated with large grains applies to fuel with the Al-Si-O additive and further implies that the release is not affected by the grain boundary phase (see Figure 8-23 and Figure 8-24).

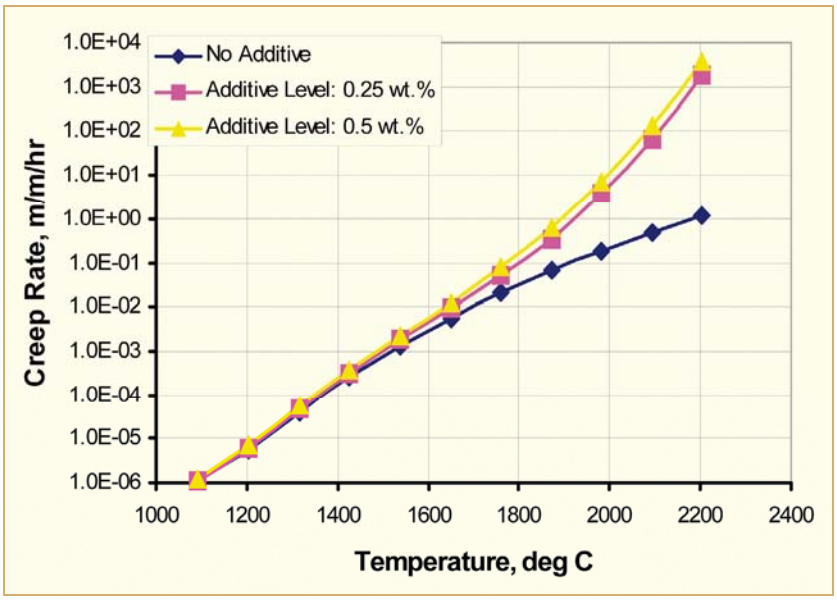

Figure 9-3: Creep of UO_2 with Al-Si-O additive under a compressive stress of 6.9 MPa relative to temperature [Davies et al, 1999].

11 References

Adamson R. B. et al, *High Burnup Fuel Issues*, ZIRAT8/IZNA3 Special Topics Report, ANT International, Skultuna, Sweden, 2003/2004.

Adamson R. B. et al, *Pellet-Cladding Interaction (PCI and PCMI)*, ZIRAT11/IZNA6, Special Topics Report, ANT International, Skultuna, Sweden, 2006/2007.

Adamson R. B, Garzarolli F. and Patterson C., *In-Reactor Creep of Zirconium Alloys*, ZIRAT14/IZNA9 Special Topical Report, ANT International, Skultuna, Sweden, 2009.

Agarwal, R., Sen, B. and Venugopal, V., *Phase diagram analysis of $(U,Pu)O_{2-x}$ sub-system*, Journal of Nuclear Materials, Vol. 385, pp. 112–116, 2009.

Ainscough J., Oldfield B. W. and Ware J. O., *Isothermal grain growth kinetics in sintered UO_2 pellets*, Journal of Nuclear Materials, Vol. 49, pp. 117-128, 1973.

Argonne National Laboratory, *Properties for LMFBR safety analysis*, ANL Report ANL-CEN-RSD-76-1, 1976.

ASTM Standard C1198-09, *Standard Test Method for Dynamic Young's Modulus, Shear Modulus and Poisson's Ratio for Advanced Ceramics by Sonic Resonance*, ASTM International, West Conshohocken, PA, USA, 2009.

Anselin F., *The Role of Fission Products in the Swelling of Irradiated UO_2 and $(U,Pu)O_2$ Fuel*, General Electric, GEAP-5583, January 1969.

Arborelius J., et al., *Advanced Doped UO_2 Pellets in LWR Applications*, Proceedings of the 2005 Water Reactor Fuel Performance Meeting, Kyoto, Japan, paper 1099, 2005.

Baichi M., Chatillon C., Ducros G. and Froment K., *Thermodynamics of the O-U System: III – Critical assessment of phase diagram data in the $U\text{-}UO_{2+x}$ composition range*, Journal of Nuclear Materials, Vol. 349, pp. 57-82, 2006.

Bailly H., Menessier D. and Prunier C., *The nuclear fuel of pressurized water reactors and fast neutron reactors*, Collection du Commissariat a l'Energie Atomic, ISBN: CEA 2-7272-0198-2, 1999.

Baldock P., Spindler W. and Baker T., *The X-ray thermal expansion of near - stoichiometric UO_2*, Journal of Nuclear Materials, Vol. 18, pp. 305-313, 1966.

Baron, D., *Fuel Thermal Conductivity: A Review of the Modelling Available for UO2, $(U\text{-}Gd)O_2$ and MOX Fuel*, Proceedings of the Seminar on Thermal Performance of High Burn-up LWR Fuel, CEA, Cadarache, France, 3-6 March 1998, pp. 129-144, 1998.

Bentejac F. et al, *Fuel Rod Modeling During Transients: The TOUTAIS Code*, Proceedings, Nuclear fuel behaviour modelling at high burnup and its experimental support, Windemere, UK, 19-23 June 2000, IAEA TECDOC-1233, 2001.

Booth A., *A Method of Calculating Fission Gas diffusion from UO_2 Fuel and Its Application to the X-2-f Loop Test*, AECL Report CRDC-721, 1957.

Bibilashvili Yu., et al., *Investigation of Thermal-Physical and Mechanical Properties of Uranium-Gadolinium Oxide Fuel*, IAEA TECDOC-1416, pp. 85-99, 2003.

Brett N. and Russell L., *The thermal expansion of PuO_2 and some other actinide oxides between room temperature and 1000 °C*, in Plutonium 1960, p. 397-410,. E. Grison, W. B. H. Lord, and R. D. Fowler, eds., Cleaver Hyne Press Ltd., London, 1961.

Brochard J., et al., *Modelling of Pellet Cladding Interaction in PWR Fuel*, Structural Mechanics in Reactor Technology, SMiRT 16, Washington, DC, USA, 2001.

Burdick M. and Parker H., *Effect of Particle Size on Bulk Density and Strength Properties of Uranium Dioxide Specimens*, Journal of the American Ceramic Society, Vol. 39, pp. 181-187, 1956.

Canon R., Roberts J. and Beals R., *Deformation of UO_2 at high temperatures*, Journal of the American Ceramics Society, Vol. 54, pp 105-112, 1971.

Carol J., Gomme R. and Leech N., *Thermal Diffusivity Measurements on Unirradiated Archive Fuel, and Fuel Irradiated in the Halden IFA-558 Experiment*, Enlarged HPG Meeting on High Burn-up Fuel Performance, Safety and Reliability and Degradation of In-core Materials and Water Chemistry Effects and Man-machine Systems Research, Paper HPR345/13, Bolskesjø, Norway, 1994.

Christensen J., *Thermal expansion and change in volume of uranium dioxide on melting*, Journal of the American Ceramic Society, Vol. 46, pp. 607-608, 1963.

Chubb W., Storhok V. W. and Keller D. L., *Observations relating to the mechanisms of swelling and gas release in UO_2 of high temperatures*, Journal of Nuclear Materials, Vol. 44, pp. 136-152, 1972.

Conway J., Fincel R. and Hein R., The *Thermal Expansion and Heat Capacity of UO_2 to 2200 °C*, Transactions of the American Nuclear Society, Vol. 6, p. 153, 1963.

Davies J. et al, *Irradiation Tests to Characterize the PCI Failure Mechanism*, Proceedings of the ANS Topical Meeting on Water Reactor Fuel Performance, St. Charles, IL, pp. 230, 1977.

Davies J., Vaidyanathan S., and Rand R., *Modified UO_2 fuel for high burnups*, TopFuel 1999, Avignon, France, pp. 385-395, 1999.

Delafoy Ch. et al, *Advanced UO_2 fuel with improved PCI resistance and fission gas retention Capability, TopFuel*, Proc. Int. Conf. Würzburg, Germany, 2003.

Delafoy C. and Dewes P., *AREVA NP new UO_2 fuel development and qualification for LWRs applications*, TopFuel-2006, Salamanca, Spain, 2006.

Delafoy C., Dewes P. and Miles T., *AREVA NP Cr_2O_3-Doped Fuel Development for BWRs*, Proceedings of the 2007 International LWR Fuel Performance Meeting, San Francisco, California, USA, paper 1071, 2007.

Duriez C., Alessandri J-P, Gervais T and Philipponneau Y., *Thermal conductivity of hypostoichiometric low Pu content (U,Pu)O_{2-x} mixed oxide*, Journal of Nuclear Materials, Vol. 277, pp. 143-158, 2000.

England, T. and Rider, B., *Evaluation and Compilation of Fission Product Yields*, Los Alamos National Laboratory, Report LA-UR-94-3106, ENDF-349, 1994.

Fink J., *Review: Thermo-physical properties of uranium dioxide*, Journal of Nuclear Materials, Vol. 279, pp 1-18, 2000.

Fujibayashi et al., IAEA Specialist Meeting on Examination of Fuel Assemblies for Water Cooled Power Reactors, Tokyo, Japan, 1981.

Garzarolli F., Von Jan R. and Stehle H., *The main causes of fuel element failure in water cooled power reactors*, Atomic Energy Review, Vol. 17, pp. 31-128, 1979.

Glasstone S. and Sesonske A., *Nuclear Reactor Engineering*, Van Nostrand Reinhold Company, New York, 1967.

Goll W. et al, *UO_2 Fuel Behavior at Rod Burn-ups to 105 MWd/kgHM*, Meeting on Status of Fuel Development and Design Methods, FZ Rossendorf, Dresden, Germany, March 2006.